THE OPERATING DIAGRAM FOR A TWO-STEP ANAEROBIC DIGESTION MODEL A PREPRINT

Tewfik Sari, Boumediene Benyahia

THE OPERATING DIAGRAM FOR A TWO-STEP ANAEROBIC DIGESTION MODEL

Tewfik Sari
ITAP, Univ Montpellier,
INRAE, Institut Agro, Montpellier, France
`tewfik.sari@inrae.fr`

Boumediene Benyahia
Laboratoire d'Automatique de Tlemcen,
Université de Tlemcen, Tlemcen, Algeria
`b.benyahia.ut1@gmail.com`

April 28, 2020

ABSTRACT

The Anaerobic Digestion Model No. 1 (ADM1) is a complex model which is widely accepted as a common platform for anaerobic process modeling and simulation. However, it has a large number of parameters and states that hinder its analytical study. Here, we consider the two-step reduced model of anaerobic digestion (AM2) which is a four-dimensional system of ordinary differential equations. The AM2 model is able to adequately capture the main dynamical behavior of the full anaerobic digestion model ADM1 and has the advantage that a complete analysis for the existence and local stability of its steady states is available. We describe its operating diagram, which is the bifurcation diagram which gives the behavior of the system with respect to the operating parameters represented by the dilution rate and the input concentrations of the substrates. This diagram, is very useful to understand the model from both the mathematical and biological points of view.

Keywords Anaerobic digestion · ADM1 · AM2 · Steady state analysis · Operating diagram · Bifurcation analysis

1 Introduction

The anaerobic digestion is a complex process in which organic material is converted into biogas (methane) in an environment without oxygen. Anaerobic digestion enables the water industry to treat waste water as a resource for generating energy and recovering valuable by-products. The complexity of the anaerobic digestion process has motivated the development of complex models, such as the widely used Anaerobic Digestion Model No. 1 (ADM1) [6]. This model has a large number of state variables and parameters. It is impossible to obtain an analytical characterization of the steady states and to describe the operating diagram, that is to say, to identify the asymptotic behaviour of existing steady-states as a function of chemostat operating parameters (substrates inflow concentrations and dilution rate). To the knowledge author, only numerical investigations are available [9].

Due to the analytical intractability of the full ADM1, work has been made towards the construction of simpler models that preserve biological meaning whilst reducing the computational effort required to find mathematical solutions of the model equations, to obtain a better understanding of the anaerobic digestion process. The most simple model of the chemostat with only one biological reaction, where one substrate is consumed by one microorganism is well understood [19, 22, 29]. However such models are too simple to encapsulate the essence of the anaerobic digestion process.

More realistic models of anaerobic digestion are two-step models, with a cascade of two biological reactions, where one substrate S_1 is consumed by one microorganism X_1, to produce a product S_2 that serves as the main limiting substrate for a second microorganism X_2 as schematically represented by the following reaction scheme:

$$k_1 S_1 \xrightarrow{\mu_1} X_1 + k_2 S_2, \quad k_3 S_2 \xrightarrow{\mu_2} X_2 + k_4 \mathrm{CH}_4 \tag{1}$$
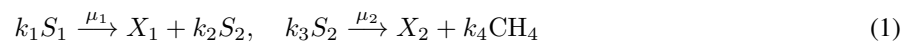
where μ_1 and μ_2 are the kinetics of the reactions and k_i are pseudo-stoichiometric coefficients associated to the bioreactions. An important contribution on the modelling of anaerobic digestion as a two-step is presented by Bernard

et al. [8], hereafter denoted as AM2. The model has a Monod kinetics for the first reaction and a Haldane one for the second and was extended with general growth functions characterized by qualitative properties by Benyahia et al. [7] and Sbarciog et al. [28]. It has been shown by García-Diéguez et al. [16] that under some circumstances, this very simple two-step model is able to adequately capture the main dynamical behavior of the full anaerobic digestion model ADM1. Moreover, it has been shown that the reduced AM2 model can support on-line control, optimization and supervision strategies, through the synthesis of state observers and control feedback laws, see for instance[2, 3].

Another simple two-step model of anaerobic digestion is the model presented by Xu et al. [35], where the product of the first microorganism, that serves as the substrate for the second microorganism, inhibits the growth of the first microorganism. The model incorporates a Monod with product inhibition kinetics for he first reaction and Monod kinetics for the second one and was extended with general growth functions characterized by qualitative properties by Daoud et al. [11] and Sari and Harmand [26].

The two-step models studied in [7, 8, 28] present a commensalistic relationship between the microorganisms. According to Stephanopolous [30], the commensalism is characterized by the fact that the second population (the commensal population) benefits for its growth from the first population (the host population) while the host population is not affected by the growth of the commensal population and hence, the first population can grow without the second one. On the contrary, the two-step models studied in [11, 26, 35] present a syntrophic relationship between the microorganisms: the first population is affected by the growth of the second population, and hence no population can grow without the other. For more details and information on commensalism and syntrophy the reader is referred to [10, 13, 24, 25, 26, 30, 31] and the references therein.

Another important and interesting extensions of the two-step anaerobic digestion models are the mathematical models, which include syntrophy and substrate inhibition, considered by Weedermann et al. [33, 34] and the three-step models, which consist in introducing an additional microorganism and substrate in a two-step syntrophic model, considered by Wade et al. [32] and Sari and Wade [27].

In this paper we will consider the two-step model of Bernard et al. [8], with general growth functions as in [7, 28], denoted here after AM2, and we describe its *operating diagram*. The operating diagram has the *operating parameters* as its coordinates and the various regions defined in it correspond to qualitatively different asymptotic behavior. A two-step model has three operating parameters that are the input concentration of substrate for each reaction and the dilution rate. These parameters are *control parameters* since they are under the control of the experimenter. Apart from these three parameters, that can vary, all other parameters have biological meaning and are fixed depending on the organisms and substrate considered.

Therefore the operating diagram is the bifurcation diagram that shows how the system behaves when we vary the control parameters. As it was claimed by Smith and Waltman in their monography on the mathematical theory of the chemostat (see [29], p. 252), the operating diagram is probably the most useful answer for the discussion of the behavior of the model with respect of the parameters. This diagram shows how robust or how extensive is the parameter region where some asymptotic behavior occur.

This bifurcation diagram is very useful to understand the model from both the mathematical and biological points of view. Its importance for ecological modeling was emphasized by De Freitas et al. [15] and for bioreactors by Pavlou [23]. These authors attributed its introduction to Jost et al. [20], who studied the dynamics of predator and prey interactions in a chemostat. This diagram is often constructed both in the biological literature [15, 20, 23, 28, 32, 35] and the mathematical literature [1, 4, 9, 11, 12, 14, 19, 21, 26, 27, 33, 34].

The operating diagram of the AM2 model was only partially described by Sbarciog et al. [28]. In this paper we give a complete description of the diagram. AM2 model can have up to six steady state. Its operating diagram presents nine regions according to the steady state and their stability, that can exist in each region. The operating diagram summarizes the effect of the operating conditions on the long-term dynamics of the AM2 model and shows six type of behavior visualized in the figures by six different colors. Since AM2 model has three operating parameters, and it is not easy to visualize regions in the three-dimensional operating parameter space, two of the operating parameters are used as coordinates of the operating diagram and the effect of the third parameter are shown in a series of operating diagrams.

This paper is organized as follows: in section 2, we present the mathematical model and recall the necessary and sufficient condition of existence and local, and global stability of its steady states. Next, in section 3, we present the operating diagram in the three-dimensional operating parameters space, in sections 4 and 5 we present the operating diagrams in two-dimensional operating parameters space when one of the parameters is kept fixed. In section 6, we present some bifurcations diagram, with the dilution rate as the bifurcation parameter. Then, we conclude by discussing our results in section 7. Proofs and Tables are given in the appendix.

2　Mathematical model

We consider the AM2 model of anaerobic digestion given in [8], which takes the form of a two-step reactions (1) where, in the first step, the organic substrate S_1 is consumed by the acidogenic bacteria X_1 and produces a substrate S_2 (Volatile Fatty Acids), while, in the second step, the methanogenic population X_2 consumes S_2 and produces methane. Let D be the dilution rate, $S_{1\text{in}}$ and $S_{2\text{in}}$ the concentrations of influent substrate S_1 and S_2, respectively. The dynamical equations of the model take the form:

$$
\begin{aligned}
\dot{S}_1 &= D\left(S_{1\text{in}} - S_1\right) - k_1\mu_1\left(S_1\right)X_1, \\
\dot{X}_1 &= \left(\mu_1\left(S_1\right) - \alpha D\right)X_1, \\
\dot{S}_2 &= D\left(S_{2\text{in}} - S_2\right) + k_2\mu_1\left(S_1\right)X_1 - k_3\mu_2\left(S_2\right)X_2, \\
\dot{X}_2 &= \left(\mu_2\left(S_2\right) - \alpha D\right)X_2,
\end{aligned}
\tag{2}
$$

where k_i are pseudo-stoichiometric coefficients associated to the bioreactions and $\alpha \in [0,1]$ is a parameter allowing us to decouple the HRT (Hydraulic Retention Time) and the SRT (Solid Retention Time). In [8], the kinetics μ_1 and μ_2 are of Monod and Haldane type, respectively:

$$
\mu_1\left(S_1\right) = \frac{m_1 S_1}{K_1 + S_1}, \qquad \mu_2\left(S_2\right) = \frac{m_2 S_2}{K_2 + S_2 + \frac{S_2^2}{K_I}},
\tag{3}
$$

The mass flow of the methane production, denoted by Q_{CH_4}, is proportional to the microbial activity, see [5]:

$$
Q_{\text{CH}_4} = k_4\mu_2\left(S_2\right)X_2
$$

where k_4 is the coefficient in (1). In this model the biogas is simply a product of the biological reactions and it has no feedback on the dynamical equations (2).

Following [7, 28], we will consider (2) with general $\mathcal{C}^1$ kinetics functions μ_1 and μ_2 satisfying the following qualitative properties:

Hypothesis 1. $\mu_1(0) = 0$, $\mu_1(+\infty) = m_1$ and $\mu_1'\left(S_1\right) > 0$ for $S_1 > 0$.

Hypothesis 2. $\mu_2\left(0\right) = 0$, $\mu_2(+\infty) = 0$ and there exists $S_2^M > 0$ such that $\mu_2'\left(S_2\right) > 0$ for $0 < S_2 < S_2^M$, and $\mu_2'\left(S_2\right) < 0$ for $S_2 > S_2^M$.

As it is usual in the mathematical theory of the chemostat, see for instance [25], we can use a change of variables that reduces the pseudo-stochiometric coefficients k_i to 1. Indeed, the linear change of variables

$$
s_1 = \frac{k_2}{k_1}S_1, \quad x_1 = k_2 X_1, \quad s_2 = S_2, \quad x_2 = k_3 X_2
$$

transforms (2) into

$$
\begin{aligned}
\dot{s}_1 &= D\left(s_{1\text{in}} - s_1\right) - f_1\left(s_1\right)x_1, \\
\dot{x}_1 &= \left(f_1\left(s_1\right) - \alpha D\right)x_1, \\
\dot{s}_2 &= D\left(s_{2\text{in}} - s_2\right) + f_1\left(s_1\right)x_1 - f_2\left(s_2\right)x_2, \\
\dot{x}_2 &= \left(f_2\left(s_2\right) - \alpha D\right)x_2,
\end{aligned}
\tag{4}
$$

where

$$
s_{1\text{in}} = \frac{k_2}{k_1}S_{1\text{in}}, \quad s_{2\text{in}} = S_{2\text{in}}, \quad f_1(s_1) = \mu_1\left(\frac{k_1}{k_2}s_1\right), \quad f_2(s_2) = \mu_2(s_2)
$$

However, since the stoichiometric coefficients have their own importance for the biologist and since we are interested in giving the biologist a useful tool for the understanding of the role of the operating parameters, we do not make this reduction and we present the results in the original model (2). This model can have at most six steady states, labeled below as in [7]:

- E_1^0, where $X_1 = 0$ and $X_2 = 0$: the washout steady state where acidogenic and methanogenic bacteria are extinct.
- E_1^i $(i = 1, 2)$, where $X_1 = 0$ and $X_2 > 0$: acidogenic bacteria are washed out, while methanogenic bacteria are maintained.
- E_2^0, where $X_1 > 0$ and $X_2 = 0$: methanogenic bacteria are washed out, while acidogenic bacteria are maintained.
- E_2^i $(i = 1, 2)$, where $X_1 > 0$ and $X_2 > 0$: both acidogenic and methanogenic bacteria are maintained.

Table 1: Auxiliary functions

$S_1^*(D)$	$S_1^*(D)$ is the unique solution of equation $\mu_1(S_1) = \alpha D$ It is defined for $0 \le D < D_1$, where $D_1 = m_1/\alpha$ If $D \ge D_1$, by convention we let $S_1^*(D) = +\infty$
$S_2^{i*}(D), i = 1, 2$	$S_2^{1*}(D) < S_2^{2*}(D)$ are the solutions of equation $\mu_2(S_2) = \alpha D$ They are defined for $0 \le D \le D_2$, where $D_2 = \mu_2\left(S_2^M\right)/\alpha$ If $D = D_2$, one has $S_2^{1*}(D) = S_2^{2*}(D)$ If $D > D_2$, by convention we let $S_2^{1*}(D) = +\infty$
$H_i(D), i = 1, 2$	$H_i(D) = S_2^{i*}(D) + \frac{k_2}{k_1}S_1^*(D)$ It is defined for $0 \le D < \min(D_1, D_2)$
$S_{2\text{in}}^*(D, S_{1\text{in}}, S_{2\text{in}})$	$S_{2\text{in}}^*(D, S_{1\text{in}}, S_{2\text{in}}) = S_{2\text{in}} + \frac{k_2}{k_1}(S_{1\text{in}} - S_1^*(D))$ It is defined for $0 \le D < D_1$ and $S_{1\text{in}} > S_1^*(D)$
$X_1^*(D, S_{1\text{in}})$	$X_1^*(D, S_{1\text{in}}) = \frac{1}{k_1\alpha}(S_{1\text{in}} - S_1^*(D))$ It is defined for $0 \le D < D_1$ and $S_{1\text{in}} > S_1^*(D)$
$X_2^i(D, S_{2\text{in}}), i = 1, 2$	$X_2^i(D, S_{2\text{in}}) = \frac{1}{k_3\alpha}(S_{2\text{in}} - S_2^{i*}(D))$ It is defined for $0 \le D < D_2$ and $S_{2\text{in}} > S_2^{i*}(D)$
$X_2^{i*}(D, S_{1\text{in}}, S_{2\text{in}}), i = 1, 2$	$X_2^{i*}(D, S_{1\text{in}}, S_{2\text{in}}) = \frac{1}{k_3\alpha}(S_{2\text{in}}^*(D, S_{1\text{in}}, S_{2\text{in}}) - S_2^{i*}(D))$ It is defined for $0 \le D < \min(D_1, D_2)$, $S_{1\text{in}} > S_1^*(D)$ and $S_{2\text{in}} + \frac{k_2}{k_1}S_{1\text{in}} > H_i(D)$

For the description of the steady states, we need to define some auxiliary functions that are given in Table 1. For the particular case of Monod and Haldane functions (3), the auxiliary functions can be computed analytically and are given in Table 14. We have the following result.

Proposition 1. *Assume that Hypotheses 1 and 2 hold. The steady states E_1^0, E_1^i ($i = 1, 2$), E_2^0 and E_2^i ($i = 1, 2$) are given in Table 2, where S_1^*, S_2^{i*}, $S_{2\text{in}}^*$, X_1^*, X_2^i, and X_2^{i*}, for $i = 1, 2$, are defined in Table 1. Their conditions of existence and stability are given in Table 3.*

Proof. The proof is given in Appendix A.1. □

Table 2: The steady states of (2). S_1^*, S_2^{i*}, $S_{2\text{in}}^*$, X_1^*, X_2^i and X_2^{i*} are defined in Table 1.

E_1^0	$S_1 = S_{1\text{in}}$	$S_2 = S_{2\text{in}}$	$X_1 = 0$	$X_2 = 0$
$E_1^i, i = 1, 2$	$S_1 = S_{1\text{in}}$	$S_2 = S_2^{i*}$	$X_1 = 0$	$X_2 = X_2^i$
E_2^0	$S_1 = S_1^*$	$S_2 = S_{2\text{in}}^*$	$X_1 = X_1^*$	$X_2 = 0$
$E_2^i, i = 1, 2$	$S_1 = S_1^*$	$S_2 = S_2^{i*}$	$X_1 = X_1^*$	$X_2 = X_2^{i*}$

Table 3: Necessary and sufficient conditions of existence and local stability of steady states of (2). $S_1^*(D)$, $S_2^{i*}(D)$ and $H_i(D)$ are defined in Table 1.

	Existence conditions	Stability conditions
E_1^0	Always exists	$S_{1\text{in}} < S_1^*(D)$ and $S_{2\text{in}} \notin \left[S_2^{1*}(D), S_2^{2*}(D)\right]$
E_1^1	$S_{2\text{in}} > S_2^{1*}(D)$	$S_{1\text{in}} < S_1^*(D)$
E_1^2	$S_{2\text{in}} > S_2^{2*}(D)$	Unstable if it exists
E_2^0	$S_{1\text{in}} > S_1^*(D)$	$S_{2\text{in}} + \frac{k_2}{k_1}S_{1\text{in}} \notin [H_1(D), H_2(D)]$
E_2^1	$S_{1\text{in}} > S_1^*(D)$ and $S_{2\text{in}} + \frac{k_2}{k_1}S_{1\text{in}} > H_1(D)$	Stable if it exists
E_2^2	$S_{1\text{in}} > S_1^*(D)$ and $S_{2\text{in}} + \frac{k_2}{k_1}S_{1\text{in}} > H_2(D)$	Unstable if it exists

Remark 1. *In Table 3, since the function S_1^* is defined on $(0, D_1)$, the condition $S_{1\text{in}} > S_1^*(D)$ means $0 < D < D_1$ and $S_{1\text{in}} > S_1^*(D)$. Conversely, since by convention $S_1^*(D) = +\infty$ for $D \ge D_1$, the condition $S_{1\text{in}} < S_1^*(D)$ means $D \ge D_1$ and $S_{1\text{in}} > 0$ or $0 < D < D_1$ and $0 < S_{1\text{in}} < S_1^*(D)$. On the other hand, since the function S_2^{i*} is defined on $(0, D_2)$, the condition $S_{2\text{in}} > S_2^{i*}(D)$ means $0 < D < D_2$ and $S_{2\text{in}} > S_2^{i*}(D)$ and, conversely, since by convention $S_2^{1*}(D) = +\infty$ for $D > D_2$, the condition $S_{2\text{in}} \notin \left[S_2^{1*}(D), S_2^{2*}(D)\right]$ means $D \ge D_2$ and $S_{2\text{in}} > 0$ or $0 < D < D_2$*

and $S_{2\text{in}} \notin \left[S_2^{1*}(D), S_2^{2*}(D) \right]$. *Similar remarks can be made concerning the conditions involving functions* $H_i(D)$, $i = 1, 2$.

3   Operating diagram

Let us consider the surfaces Γ_i, $i = 1 \cdots 6$, defined by Table 4. Notice that $S_2^{1*}(D) < S_2^{2*}(D)$ for $0 < D < D_2$ and equality holds for $D = D_2$. Similarly $H_1(D) < H_2(D)$ for $0 < D < \min(D_1, D_2)$, and equality holds for $D = \min(D_1, D_2)$. Therefore, the Γ_i surfaces separate the operating space $(D, S_{1\text{in}}, S_{2\text{in}})$ into nine regions, denoted $\mathcal{I}_k$, $k = 0 \cdots 8$, and defined in Table 5. These regions of the operating parameters space $(D, S_{1\text{in}}, S_{2\text{in}})$ are corresponding to different system behaviors, as stated in the following result.

Table 4: The surfaces Γ_i, $i = 1 \cdots 6$.

$\Gamma_1 = \left\{ (D, S_{1\text{in}}, S_{2\text{in}}) : 0 < D < D_1 \text{ and } S_{1\text{in}} = S_1^*(D) \right\}$
$\Gamma_2 = \left\{ (D, S_{1\text{in}}, S_{2\text{in}}) : 0 < D < D_2 \text{ and } S_{2\text{in}} = S_2^{1*}(D) \right\}$
$\Gamma_3 = \left\{ (D, S_{1\text{in}}, S_{2\text{in}}) : 0 < D < D_2 \text{ and } S_{2\text{in}} = S_2^{2*}(D) \right\}$
Notice that
$\qquad \Gamma_1 = \left\{ (D, S_{1\text{in}}, S_{2\text{in}}) : S_{1\text{in}} > 0 \text{ and } \alpha D = \mu_1(S_{1\text{in}}) \right\}$
$\qquad \Gamma_2 \cup \Gamma_3 = \left\{ (D, S_{1\text{in}}, S_{2\text{in}}) : S_{2\text{in}} > 0 \text{ and } \alpha D = \mu_2(S_{2\text{in}}) \right\}$
$\Gamma_4 = \left\{ (D, S_{1\text{in}}, S_{2\text{in}}) : 0 < D < \min(D_1, D_2), S_{1\text{in}} > S_1^*(D) \text{ and } S_{2\text{in}} + \frac{k_2}{k_1} S_{1\text{in}} = H_1(D) \right\}$
$\Gamma_5 = \left\{ (D, S_{1\text{in}}, S_{2\text{in}}) : 0 < D < \min(D_1, D_2), S_{1\text{in}} > S_1^*(D) \text{ and } S_{2\text{in}} + \frac{k_2}{k_1} S_{1\text{in}} = H_2(D) \right\}$
$\Gamma_6 = \left\{ (D, S_{1\text{in}}, S_{2\text{in}}) : D = D_2 \right\}$

Table 5: Definitions of the nine regions corresponding to the nine cases in [7].

Case of [7]	Region	Definition
1.1	$\mathcal{I}_0$	$S_{1\text{in}} < S_1^*(D)$ and $S_{2\text{in}} < S_2^{1*}(D)$
1.2	$\mathcal{I}_1$	$S_{1\text{in}} < S_1^*(D)$ and $S_2^{1*}(D) < S_{2\text{in}} \leq S_2^{2*}(D)$
1.3	$\mathcal{I}_2$	$S_{1\text{in}} < S_1^*(D)$ and $S_{2\text{in}} > S_2^{2*}(D)$
2.1	$\mathcal{I}_3$	$S_{1\text{in}} > S_1^*(D)$ and $S_{2\text{in}} + \frac{k_2}{k_1} S_{1\text{in}} < H_1(D)$
2.2	$\mathcal{I}_4$	$S_{1\text{in}} > S_1^*(D)$, $S_{2\text{in}} \leq S_2^{1*}(D)$ and $H_1(D) < S_{2\text{in}} + \frac{k_2}{k_1} S_{1\text{in}} \leq H_2(D)$
2.3	$\mathcal{I}_5$	$S_{1\text{in}} > S_1^*(D)$, $S_{2\text{in}} \leq S_2^{1*}(D)$ and $S_{2\text{in}} + \frac{k_2}{k_1} S_{1\text{in}} > H_2(D)$
2.4	$\mathcal{I}_6$	$S_{1\text{in}} > S_1^*(D)$, $S_{2\text{in}} > S_2^{1*}(D)$ and $S_{2\text{in}} + \frac{k_2}{k_1} S_{1\text{in}} \leq H_2(D)$
2.5	$\mathcal{I}_7$	$S_{1\text{in}} > S_1^*(D)$, $S_2^{1*}(D) < S_{2\text{in}} \leq S_2^{2*}(D)$ and $S_{2\text{in}} + \frac{k_2}{k_1} S_{1\text{in}} > H_2(D)$
2.6	$\mathcal{I}_8$	$S_{1\text{in}} > S_1^*(D)$ and $S_{2\text{in}} > S_2^{2*}(D)$

Proposition 2. *Assume that Hypotheses 1 and 2 hold. The existence and stability properties of the steady states of (2) are given in Table 6, where the regions* $\mathcal{I}_k$, $k = 0 \cdots 8$ *are defined in Table 5.*

Proof. The proof is given in Appendix A.2. $\qquad\qquad\qquad\qquad\qquad\qquad\qquad\qquad\qquad\qquad\qquad\qquad$ $\square$

Remark 2. *In in Figs. 3, 4, 5, 7 and 8 presenting operating diagrams, a region is colored according to the color in Table 6. Each color corresponds to different asymptotic behavior:*

- *Red for the washout of both species, that is, the steady state E_1^0 is Globally asymptotically stable (GAS), which occurs in region $\mathcal{I}_0$.*

- *Blue for the washout of acidogenic bacteria while methanogenic bacteria are maintained, that is, the steady state E_1^1 is GAS, which occurs in region $\mathcal{I}_1$.*

- *Cyan for the bistability of E_1^0 and E_1^1 which are both (locally) stable. This behavior occurs in region $\mathcal{I}_1$. Depending on the initial condition the system can go to the washout of both species or the washout of only the acidogenic bacteria.*

- *Yellow for the washout of methanogenic bacteria while acidogenic bacteria are maintained, that is the steady state E_2^0 is GAS, which occurs in region $\mathcal{I}_3$.*

5

Table 6: Existence and stability of steady states of (2) in the nine regions of the operating space. GAS, S and U stand for *Globally asymptotically stable*, *Locally exponentially stable* and *Unstable* respectively. The last colum show the color in which the region is depiced in Figs. 3, 4, 5, 7, 8 and 9.

Region	E_1^0	E_1^1	E_1^2	E_2^0	E_2^1	E_2^2	Color
$\mathcal{I}_0$	GAS						Red
$\mathcal{I}_1$	U	GAS					Blue
$\mathcal{I}_2$	S	S	U				Cyan
$\mathcal{I}_3$	U			GAS			Yellow
$\mathcal{I}_4$	U			U	GAS		Green
$\mathcal{I}_5$	U			S	S	U	Pink
$\mathcal{I}_6$	U	U		U	GAS		Green
$\mathcal{I}_7$	U	U		S	S	U	Pink
$\mathcal{I}_8$	U	U	U	S	S	U	Pink

- *Green for the global asymptotic stability of the positive steady state E_2^1, which occur in $\mathcal{I}_4$ and $\mathcal{I}_6$. These regions differ only by the existence, in the second region, of the unstable boundary steady state E_1^1.*

- *Pink for the bistability of E_2^0 and E_2^1 which are both locally asymptotically stable. This behavior occurs in regions $\mathcal{I}_5$, $\mathcal{I}_7$ and $\mathcal{I}_8$. These regions differ only by the possible existence of the unstable boundary steady states E_1^1 or E_1^2. Depending on the initial condition the system can go to the washout of methanogenic bacteria or the coexistence of both species.*
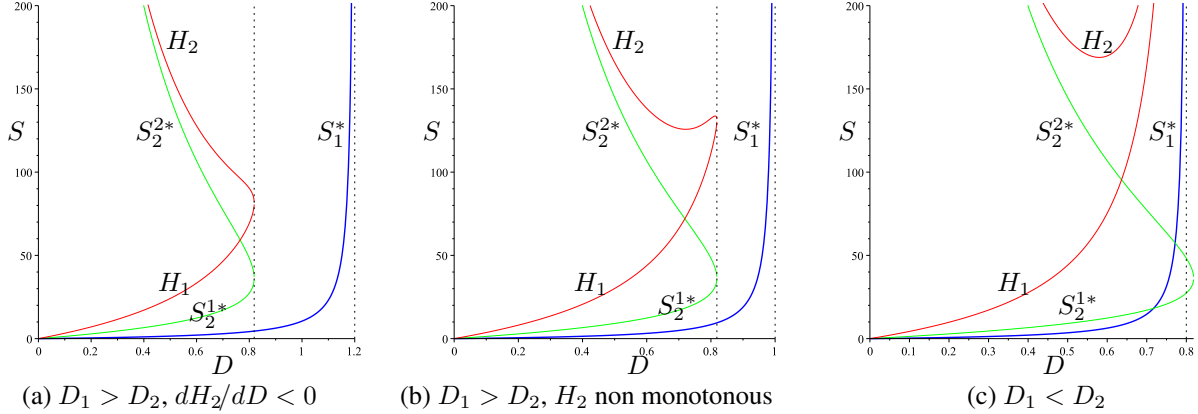

Figure 1: The graphs of functions $S = S_1^*(D)$ (in Blue), $S = S_2^{i*}(D)$, $i = 1, 2$ (in Green) and $S = H_i(D)$3, $i = 1, 2$ (in Red). (a): $m_1 = 0.6$; (b): $m_1 = 0.5$ (c): $m_1 = 0.4$. Other biological parameter values are given in Table 11. Compare with Fig. 4 of [28]

Table 7: Three behaviors for functions H_i, $i = 1, 2$

Case (A), where $D_1 > D_2$ and $dH_2/dD < 0$.
Case (B), where $D_1 > D_2$ and H_2 non monotonous.
Case (C), where where $D_1 < D_2$.

The operating diagram highly depends on the shape of Γ_4 and Γ_5 surfaces, that is to say, on the behaviors of functions H_i, $i = 1, 2$, defined in Table 1. Notice that these functions are defined on $(0, \min(D_1, D_2))$ and H_1 is increasing, since it is the sum of two increasing functions. We have

$$\lim_{D \to 0} H_1(D) = 0, \quad \lim_{D \to 0} H_2(D) = +\infty, \quad \lim_{D \to 0} \frac{dH_2}{dD}(D) = -\infty,$$

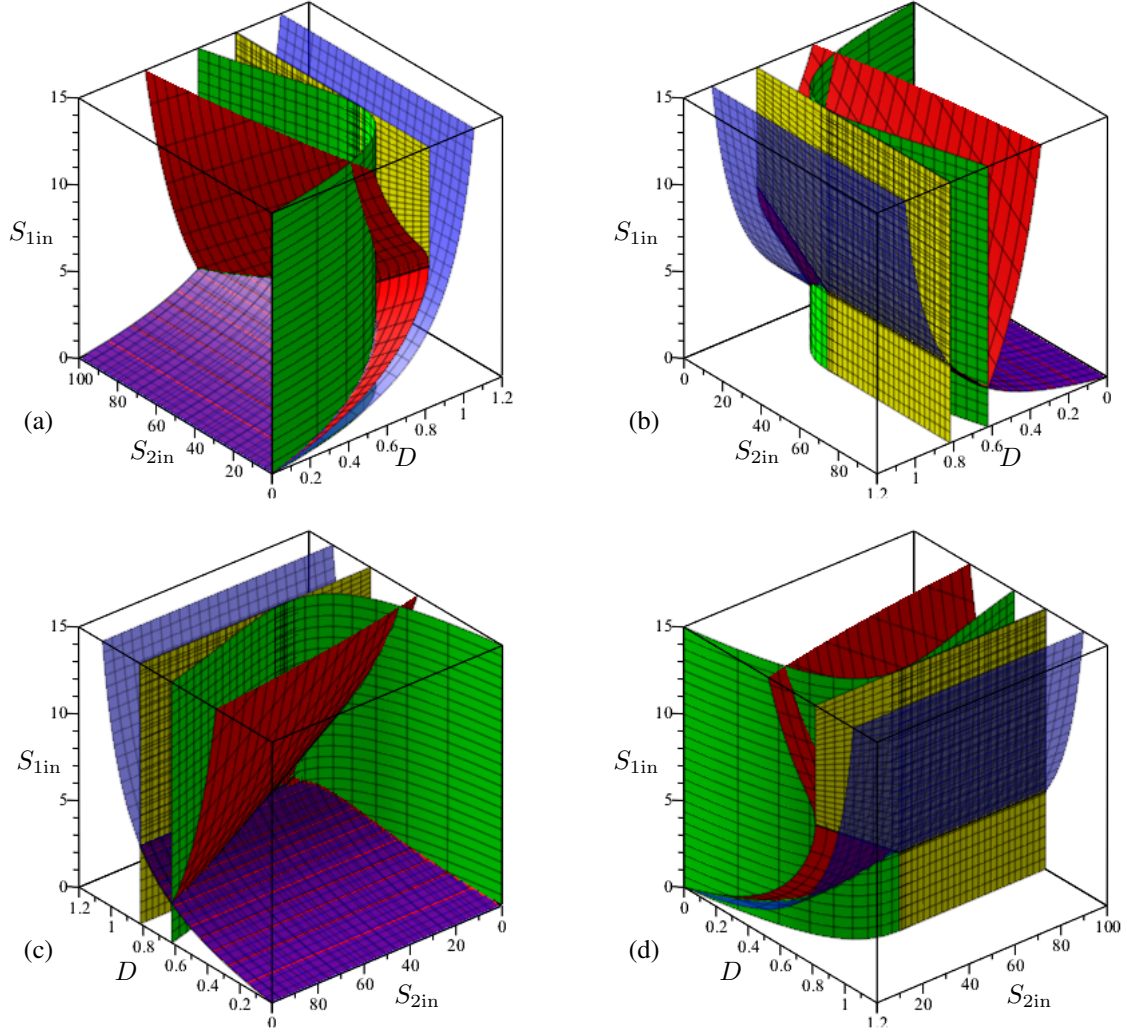For the limits at right of the domain of definition of these functions, we must distinguish two cases:

Figure 2: The surfaces Γ_1 (in Blue), Γ_2 and Γ_3 (in Green), Γ_4 and Γ_5 (in Red) and Γ_6 (in Yellow), corresponding to Fig. 1(a). The surfaces separate the 3-dimensional operating space $(D, S_{1\text{in}}, S_{2\text{in}})$ in 9 regions $\mathcal{I}_k$, $k = 0 \cdots 8$. Front (a), rear (b), left (c) and right (d) view of the surfaces Γ_i. Compare with Fig. 6 of [28].

- When $D_1 < D_2$, the functions H_i, $i = 1, 2$ are defined on $(0, D_1)$ and

$$\lim_{D \to D_1} H_1(D) = \lim_{D \to D_1} H_2(D) = +\infty,$$

- When $D_2 < D_1$, the functions H_i, $i = 1, 2$ are defined on $(0, D_2)$ and

$$\lim_{D \to D_2} H_1(D) = \lim_{D \to D_2} H_2(D) = S_2^M + \frac{k_2}{k_1} S_1^*(D_2), \quad \lim_{D \to D_2} \frac{dH_1}{dD}(D) = +\infty, \quad \lim_{D \to D_2} \frac{dH_2}{dD}(D) = -\infty.$$

  Two qualitatively different sub-cases can be distinguished: either H_2 is decreasing on $(0, D_2)$ or it is not monotonous. Since H_2 is decreasing near the extremities of its definition interval, a typical example is where it is decreasing, then increasing and then decreasing.

Therefore there are three cases summarized in Table 7 and illustrated in Fig. 1. The role of H_i-functions, in the description of the operating diagram, has already been highlighted, see Fig. 4 in [28], where cases $D_2 < D_1$ and $D_1 < D_2$ are distinguished.

Since the surfaces Γ_i, $i = 1 \cdots 6$, which are the boundaries of the various regions have been derived analytically, the operating diagrams can be drawn qualitatively in each of these cases. Instead of giving a general qualitative description

7

of the operating diagram, and without loss of generality, we present the specific examples shown in Fig. 1. These examples are obtained with the Monod and Haldane functions 3. Notice that these functions satisfy Hypotheses 1 and 2. Therefore, the results of Propositons 1 and 2 apply. The analytical expressions of the auxiliary functions defined in Table 1 and needed in the defintions of the regions $\mathcal{I}_k$ of the operating diagrams are given in Table 14, in the particular case of functions 3. The biological parameter values used in the figures are given in Table 11. For the sake of practical applicability, these parameter values were chosen in a range that can be found in the literature [7, 8].

For the biological parameter values corresponding Fig. 1(a), the surfaces Γ_i, $i = 1 \cdots 6$ are shown in Fig. 2. It is difficult to visualize the regions $\mathcal{I}_k$, $k = 0 \cdots 8$ of the three-dimensional operating diagram. We can have a better understanding of these regions by showing cuts along 2 dimensional planes where one of the operating parameters is kept constant. For instance, if D is kept constant, we obtain then the operating diagram in the 2-dimensional plane $(S_{1\text{in}}, S_{2\text{in}})$. These operating diagrams are described in section 4. If $S_{2\text{in}}$ is kept constant, we obtain then the operating diagram in the 2-dimensional plane $(D, S_{1\text{in}})$. These operating diagrams are described in section 5.
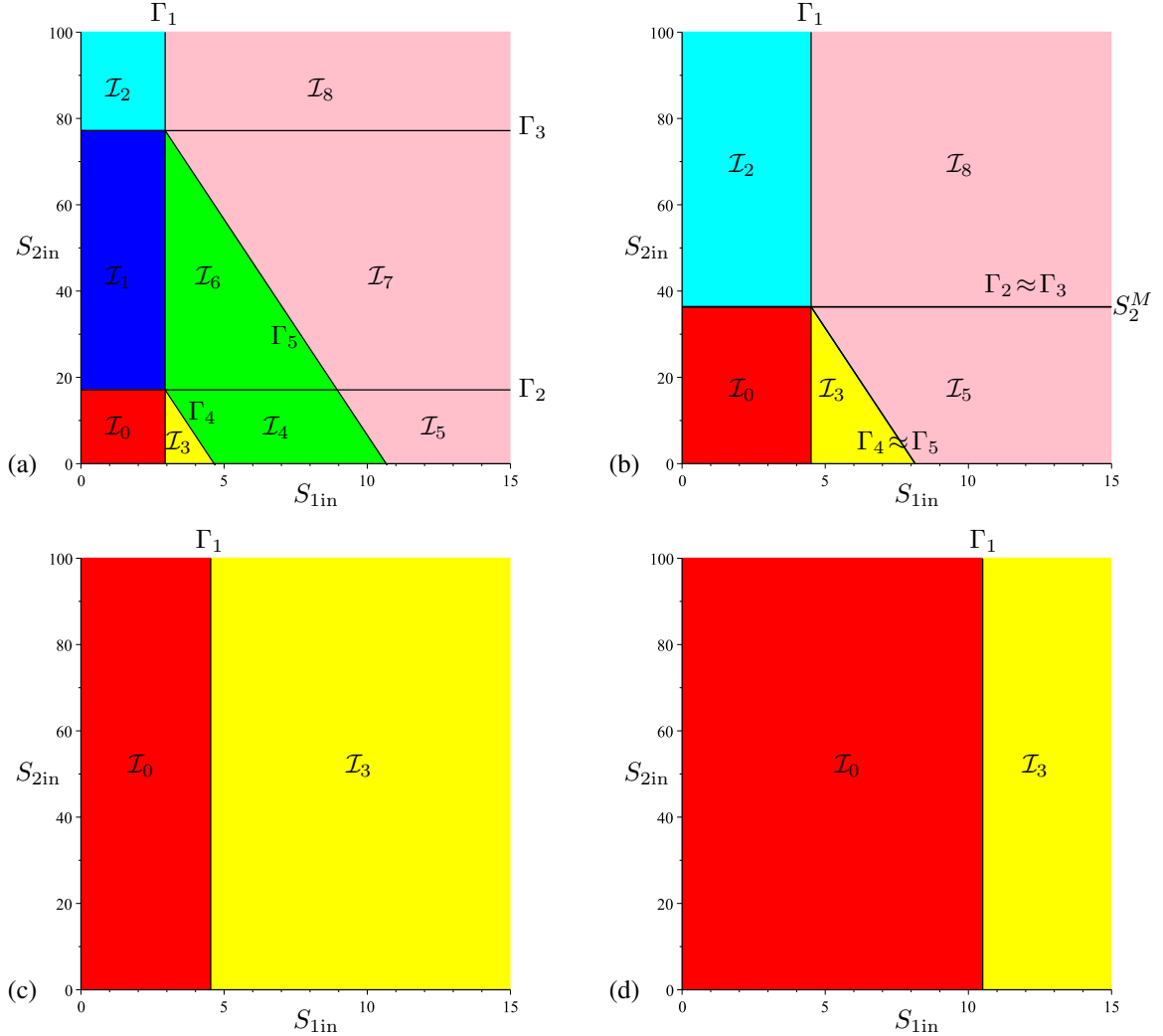

Figure 3: The 2-dimensional operating diagram $(S_{1\text{in}}, S_{2\text{in}})$ obtained by cuts at D constant of the 3-dimensional operating diagram shown in Fig. 2. (a): $D = 0.7$; (b): $D = 0.818557 < D_2$; (c): $D = 0.82 > D_2$; (d): $D = 1 < D_1$. Here $D_1 = 1.2$, $D_2 \approx 0.818557467$ and $S_2^M \approx 36.332$.

4 Operating diagram in $(S_{1\text{in}}, S_{2\text{in}})$ where D is kept constant

The intersections of the surfaces Γ_i, $i = 1 \cdots 5$ with a plane where D is kept constant are straight lines: vertical line for Γ_1, horizontal lines for Γ_2 and Γ_3 and oblique lines for Γ_4 and Γ_5, see Table 12. These straight lines separate
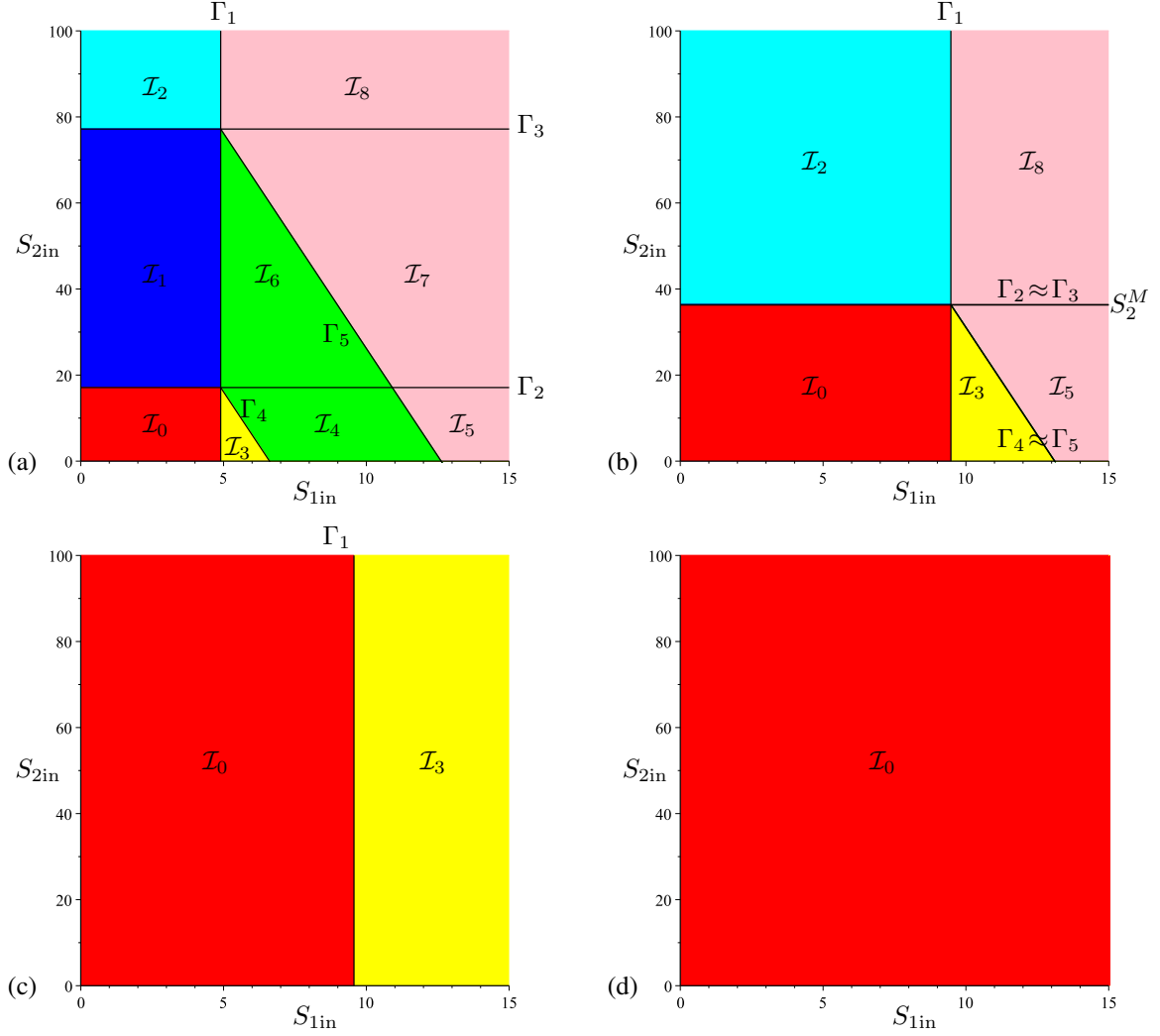
Figure 4: The 2-dimensional operating diagram $(S_{1\mathrm{in}}, S_{2\mathrm{in}})$ with D constant, corresponding to Fig. 1(b). (a): $D = 0.7$; (b): $D = 0.818557 < D_2$; (c): $D = 0.82 > D_2$; (d): $D = 1 \geq D_1$. Here $D_1 = 1$, $D_2 \approx 0.818557467$ and $S_2^M \approx 36.332$.

the operating parameter plane $(S_{1\mathrm{in}}, S_{2\mathrm{in}})$ in up to nine regions $\mathcal{I}_k$, $k = 0 \cdots 8$. Since the curves are straight lines, the regions of the operating diagram are very easy to picture. We begin by considering the case where $D_2 < D_1$ corresponding to Figs. 1(a) and 1(b).

4.1 Operating diagram when $D_2 < D_1$

The cuts at D constant of the 3-dimensional operating diagram shown in Fig. 2 and corresponding to Fig. 1(a), are shown in Fig. 3. The regions are colored according to the colors in Table 6. For the clarity of the picture all straight lines Γ_i are plotted in black. Fig. 3 shows the following features.

For $0 < D < D_2$ all regions exist, see Fig. 3(a). For increasing D, the vertical line Γ_1 defined by $S_{1\mathrm{in}} = S_1^*(D)$ moves to the right and tends towards the vertical line defined by $S_{1\mathrm{in}} = S_1^*(D_2)$. At the same time, the horizontal lines Γ_2 and Γ_3, defined by $S_{2\mathrm{in}} = S_2^{1*}(D)$ and $S_{2\mathrm{in}} = S_2^{2*}(D)$, respectively, move towards each other and tend toward the horizontal line defined by $S_{2\mathrm{in}} = S_2^M$, so that the regions $\mathcal{I}_1$, $\mathcal{I}_4$ and $\mathcal{I}_5$ shrink an disappear, see Fig. 3(b).

For $D = D_2$ the operating diagram changes dramatically, since regions $\mathcal{I}_1$, $\mathcal{I}_2$, $\mathcal{I}_4$, $\mathcal{I}_5$, $\mathcal{I}_6$, $\mathcal{I}_7$ and $\mathcal{I}_8$ disappear and regions $\mathcal{I}_0$, $\mathcal{I}_3$ invade the whole operating plan. See Figs. 3(b) and 3(c) obtained for $D = 0.818557 < D_2$ and $D = 0.82 > D_2$ respectively, where $D_2 \approx 0.818557467$.

9

For $D_2 < D < D_1$ only regions $\mathcal{I}_0$ and $\mathcal{I}_3$ appear, see Figs. 3(c) and 3(d). For increasing D, the vertical line Γ_1 defined by $S_{1\text{in}} = S_1^*(D)$ moves to the right and tends towards infinity. For $D \geq D_1$ only region $\mathcal{I}_0$ appears.

The cuts D constant of the 3-dimensional operating diagram corresponding to Fig. 1(b), are shown in Fig. 4. This figure has the same qualitative characteristics as Fig. 3: presence of all regions when $0 < D < D_2$ as shown in Fig. 4(a); disappearance of all regions except regions $\mathcal{I}_0$ and $\mathcal{I}_3$, when $D = D_2$, as shown in the transition from Fig. 4(b) to Fig. 4(c); disappearance of region $\mathcal{I}_3$, when $D \geq D_1$, as shown in 4(d).

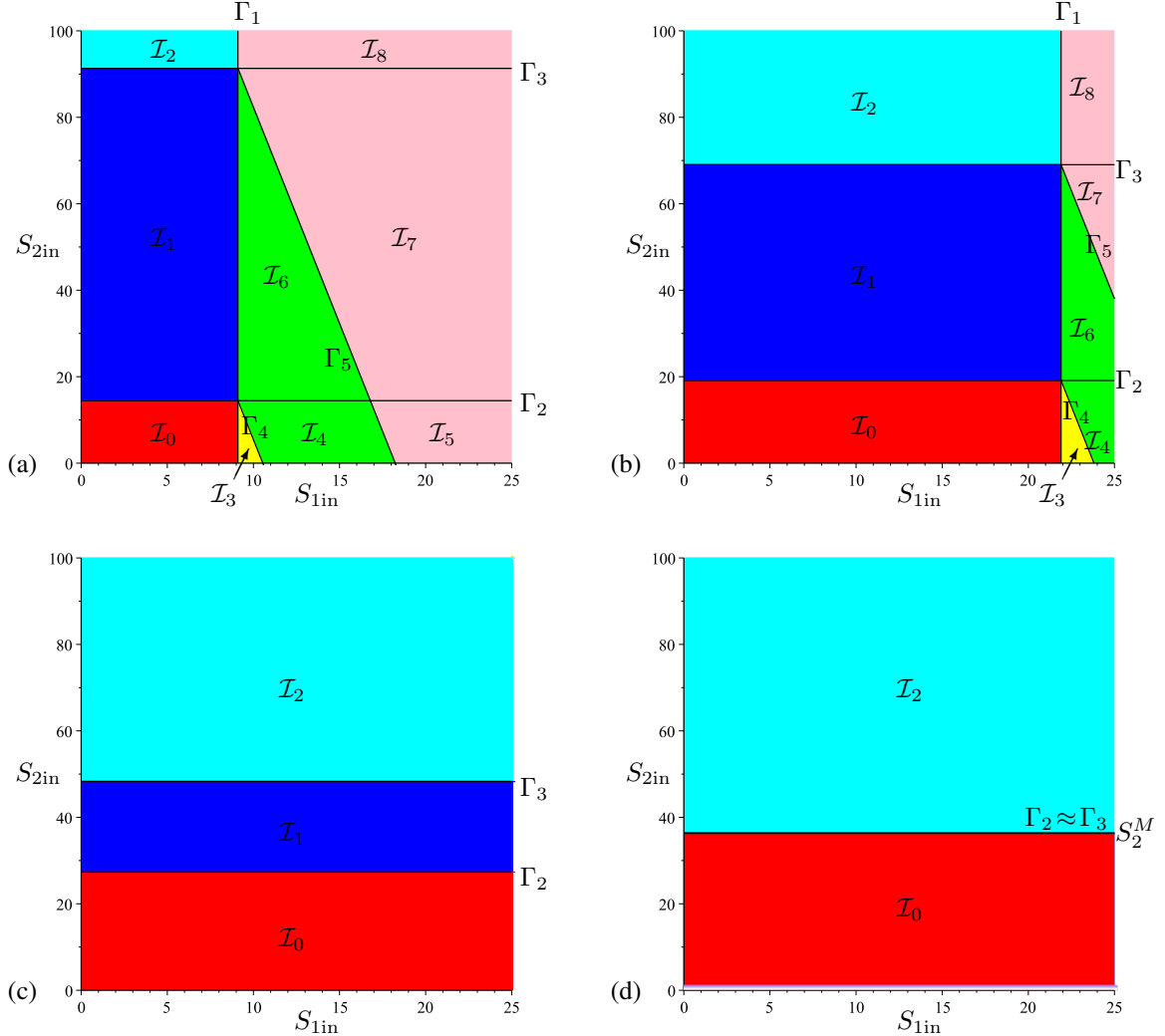## 4.2 Operating diagram when $D_1 < D_2$

Figure 5: The 2-dimensional operating diagram $(S_{1\text{in}}, S_{2\text{in}})$ with D constant, corresponding to Fig. 1(c). (a): $D = 0.65$; (b): $D = 0.73$; (c): $D = D1 = 0.8$; (d): $D = 0.818557 < D_2$. Here $D_2 \approx 0.818557467$ and $S_M^2 \approx 36.332$.

The cuts D constant of the 3-dimensional operating corresponding to Fig. 1(c), are shown in Fig. 5. The regions are colored according to the colors in Table 6. Fig. 5 shows the following features.

For $0 < D < D_1$ all regions appear, see Fig. 5(a). For increasing D, the vertical line Γ_1 defined by $S_{1\text{in}} = S_1^*(D)$ moves to the right and tends towards infinity. At the same time, the horizontal lines Γ_2 and Γ_3, defined by $S_{2\text{in}} = S_2^{1*}(D)$ and $S_{2\text{in}} = S_2^{2*}(D)$, respectively, move towards each other, as depicted in Fig. 5(b), and tend towards the horizontal lines defined by $S_{2\text{in}} = S_2^{1*}(D_1)$ and $S_{2\text{in}} = S_2^{2*}(D_1)$, respectively, as depicted in Fig. 5(c).

For $D = D_1$, the operating diagram changes dramatically: all regions $\mathcal{I}_3$, $\mathcal{I}_4$ and $\mathcal{I}_5$, $\mathcal{I}_6$, $\mathcal{I}_7$ and $\mathcal{I}_8$ have disappeared since they are located to the right of the vertical Γ_1 which tends toward infinity, when D tends to D_1, as depicted in Fig. 5(c).

For $D_1 \leq D < D_2$ only regions $\mathcal{I}_0$, $\mathcal{I}_1$, and $\mathcal{I}_2$ appear. For increasing D, the horizontal lines Γ_2 and Γ_3, defined by $S_{2in} = S_2^{1*}(D)$ and $S_{2in} = S_2^{2*}(D)$, respectively, move towards each other and tend toward the horizontal line defined by $S_{2in} = S_2^M$, so that the regions $\mathcal{I}_1$ shrinks an disappear, see Fig. 5(d).

For $D = D_2$ the operating diagram changes dramatically, since regions $\mathcal{I}_1$ and $\mathcal{I}_2$ disappear and region $\mathcal{I}_0$ invades the whole operating plan. For $D \geq D_2$ only region $\mathcal{I}_0$ appears.

Figure 6: The 2-dimensional operating diagram (D, S_{1in}) obtained by cuts at S_{2in} constant of the 3-dimensional operating diagram shown in Fig. 2 and corresponding to Fig. 1(a). (a): $S_{2in} = 0$, (b): $S_{2in} = 15$, (c): $S_{2in} = S_2^M \simeq 36.332$ and (d): $S_{2in} = 100$.

5   Operating diagram in (D, S_{1in}) where S_{2in} is kept constant

The intersections of Γ_2 and Γ_3 and Γ_6 surfaces with a plane where S_{2in} is kept constant are vertical lines, and the intersections of Γ_1, Γ_4 and Γ_5 surface with this plane are curves of funtions of D, as shown in Table 13. Curves Γ_1 and Γ_6 do not depend on S_{2in} while curves Γ_2, Γ_3, Γ_4 and Γ_5 depend on S_{2in}. Note that curves Γ_4 and Γ_5 simply consist of translating downwards the H_1 and H_2 function curves, shown in Fig. 1, and multiplying by k_1/k_2. The curves
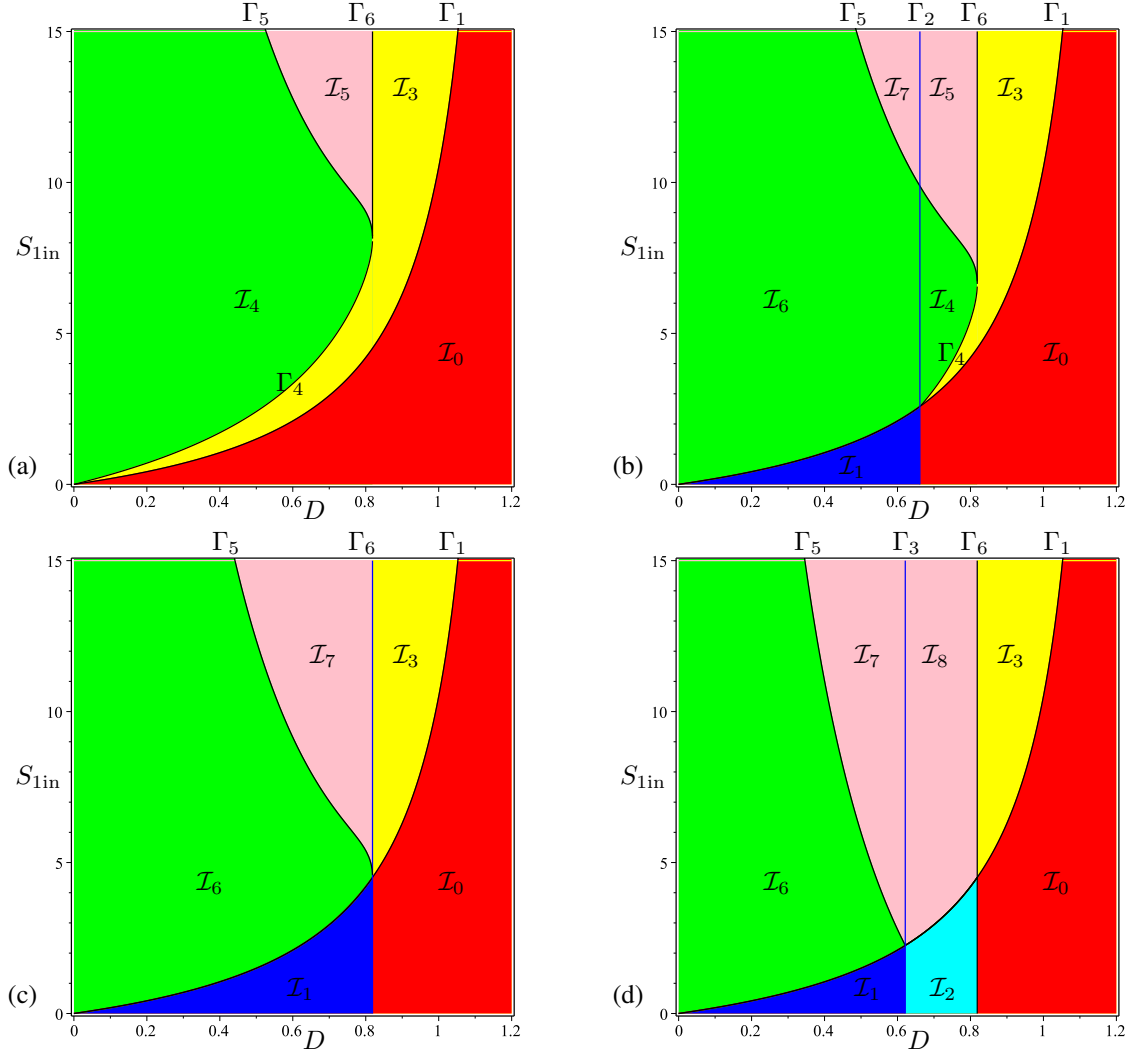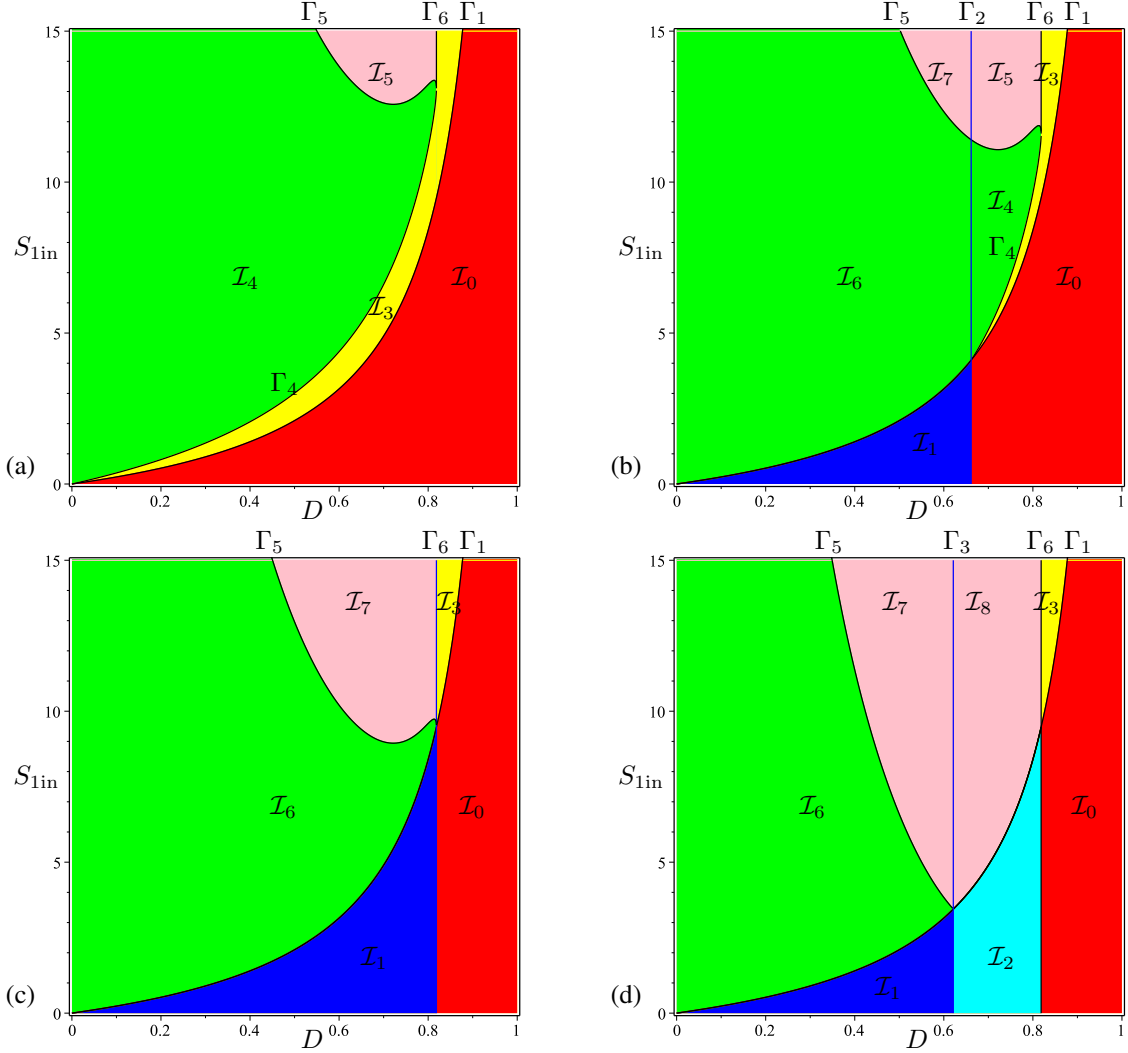
Figure 7: The 2-dimensional operating diagram $(D, S_{1\text{in}})$ obtained by cuts at $S_{2\text{in}}$ constant of the 3-dimensional operating diagram corresponding to Fig. 1(b). (a): $S_{2\text{in}} = 0$, (b): $S_{2\text{in}} = 15$, (c): $S_{2\text{in}} = S_2^M \approx 36.332$ and (d): $S_{2\text{in}} = 100$.

Γ_k, $k = 1 \cdots 6$, separate the operating parameter plane $(D, S_{1\text{in}})$ in up to nine regions $\mathcal{I}_k$, $k = 0 \cdots 8$. We begin by considering the case where $D_2 < D_1$ corresponding to Figs. 1(a) and 1(b).

5.1   Operating diagram when $D_2 < D_1$

The cuts at $S_{2\text{in}}$ constant of the 3-dimensional operating diagram shown in Fig. 2 and corresponding to Fig. 1(a), are shown in Fig. 6. The regions are colored according to the colors in Table 6. Fig. 6 shows the following features.

For $S_{2\text{in}} = 0$, only the regions $\mathcal{I}_0$, $\mathcal{I}_3$, $\mathcal{I}_4$ and $\mathcal{I}_5$ exist, see Fig. 6(a). For $0 < S_{2\text{in}} < S_2^M$, Γ_2 curve appears, giving birth to $\mathcal{I}_1$, $\mathcal{I}_6$ and $\mathcal{I}_7$ regions, see Fig. 6(b). For increasing $S_{2\text{in}}$, Γ_4 and Γ_5 curves are translated downwards, while the vertical line Γ_2 moves to the right and tends towards the vertical line Γ_6, as $S_{2\text{in}}$ tends to S_2^M.

For $S_{2\text{in}} = S_2^M$, Γ_4 curve disappears, while Γ_2 becomes equal to Γ_6, so that $\mathcal{I}_4$ and $\mathcal{I}_5$ regions have disappeared, see Fig. 6(c). For $S_{2\text{in}} > S_2^M$, Γ_3 curve appears, giving birth to $\mathcal{I}_2$ and $\mathcal{I}_8$ regions, see Fig. 6(d). For increasing $S_{2\text{in}}$, the vertical line Γ_3 moves to the left, while Γ_5 curve is translated downwards.

The cuts $S_{2\text{in}}$ constant of the 3-dimensional operating diagram corresponding to Fig. 1(b), are shown in Fig. 7. This figure has the same qualitative characteristics as Fig. 6: presence of only $\mathcal{I}_0$, $\mathcal{I}_3$, $\mathcal{I}_4$ and $\mathcal{I}_5$ regions when $S_{2\text{in}} = 0$, see

Fig. 7(a); appearance of $\mathcal{I}_1$, $\mathcal{I}_6$ and $\mathcal{I}_7$ regions when $0 < S_{2\text{in}} < S_2^M$, see Fig. 7(b); disappearance of $\mathcal{I}_4$ and $\mathcal{I}_5$ regions when $S_{2\text{in}} = S_2^M$, see Fig. 7(c); appearance of $\mathcal{I}_2$ and $\mathcal{I}_8$ regions when $S_{2\text{in}} > S_2^M$, see Fig. 7(d).

It should be noticed that in Fig. 7, the region of global asymptotic stability of the positive steady state E_2^1 (the Green region $\mathcal{I}_4 \cup \mathcal{I}_6$) presents the very surprising property that there exists a range of values for the operating parameters $S_{1\text{in}}$ and $S_{2\text{in}}$ such that the system can go from the bistability region (the Pink region $\mathcal{I}_5 \cup \mathcal{I}_7$), to the global asymptotic stability region, when the dilution rate D increases. Indeed, the boundary Γ_5 of Green and Pink regions has an increasing part, with respect to parameter D. Therefore, near this part of Γ_5, as $S_{1\text{in}}$ is kept constant and D increases the system goes from $\mathcal{I}_5$ to $\mathcal{I}_4$, see Fig. 7(a) and 7(b), or goes from $\mathcal{I}_7$ to $\mathcal{I}_6$, see Fig. 7(c).

This possibility of globally stabilizing the system, which presents bistability, is surprising since the global stability of the positive steady state is more likely obtained by decreasing D rather than increasing it. This unespecated behavior was first observed in a slightly different two-step model, where the first kinetics is of Contois type [17]. This behavior is investigated in [18].

It is worth-noting that this unexpected behavior can occur only for suitable values of the biological parameters. For instance, in Fig. 6, where all biological parameters are the same as in Fig. 7, excepted that m_1 is changed from $m_1 = 0.5$ to $m_1 = 0.6$, the behavior does not occur and a transition from Pink region to Green region is possible only by decreasing D.
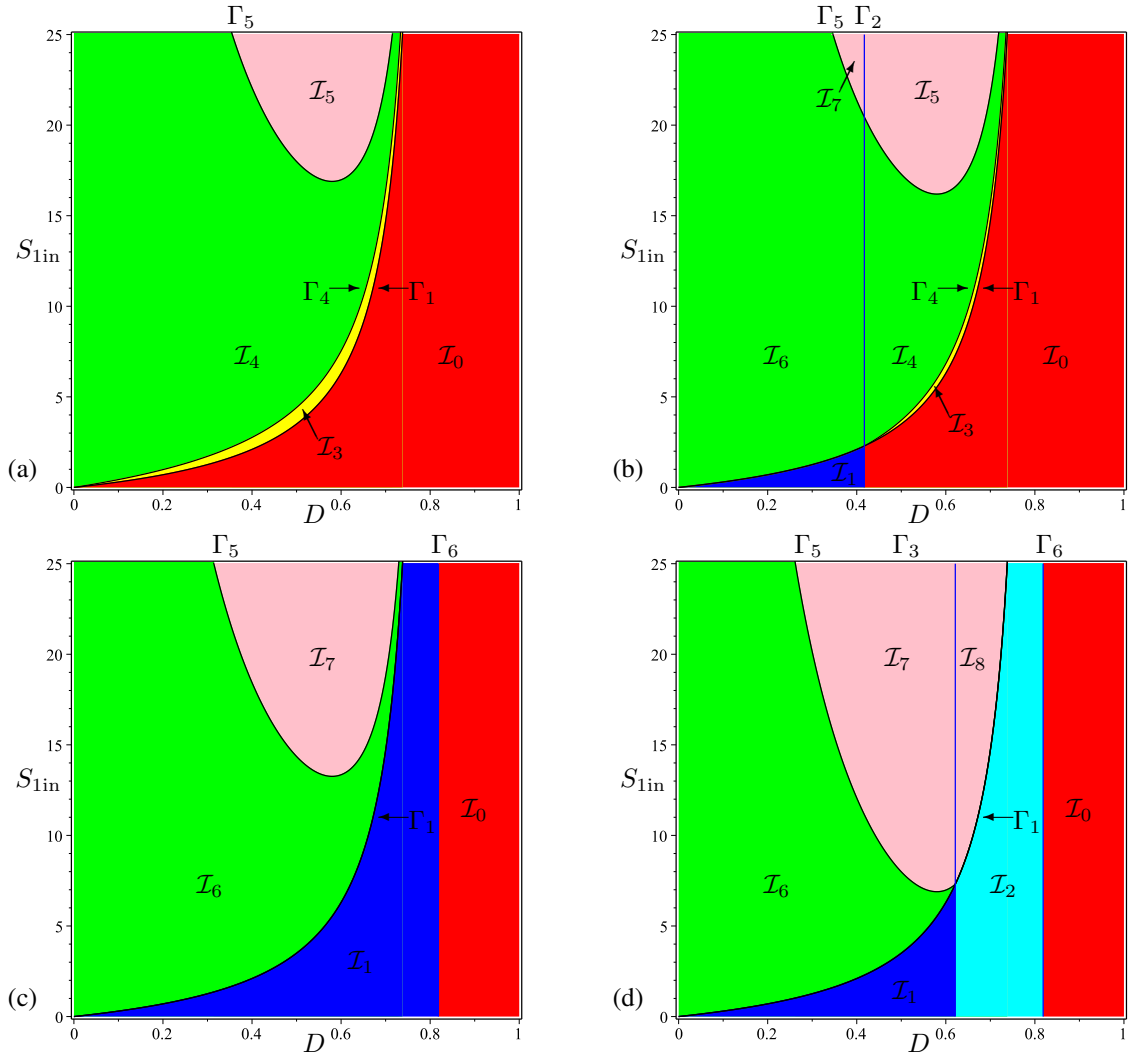

Figure 8: The 2-dimensional operating diagram $(D, S_{1\text{in}})$ obtained by cuts at $S_{2\text{in}}$ constant of the 3-dimensional operating diagram corresponding to Fig. 1(c). (a): $S_{2\text{in}} = 0$, (b): $S_{2\text{in}} = 7$, (c): $S_{2\text{in}} = S_2^M \simeq 36.3$ and (d): $S_{2\text{in}} = 100$.

5.2   Operating diagram when $D_1 < D_2$

The cuts at $S_{2\text{in}}$ constant of the 3-dimensional operating diagram corresponding to Fig. 1(c), are shown in Fig. 8. The regions are colored according to the colors in Table 6. Since $D_1 < D_2$ there exists a value $S_2^0 < S_2^M$ such that $\mu_2(S_2^0) = \alpha D_1$.

Fig. 8 shows the following features. For $S_{2\text{in}} = 0$, only regions $\mathcal{I}_0$, $\mathcal{I}_3$, $\mathcal{I}_4$ and $\mathcal{I}_5$ appear, see Fig. 8(a). For $0 < S_{2\text{in}} < S_2^0$, Γ_2 curve appears, giving birth to $\mathcal{I}_1$, $\mathcal{I}_6$, $\mathcal{I}_7$ regions, see Fig. 8(b). For increasing $S_{2\text{in}}$, Γ_4 and Γ_5 curves are translated downwards, while the vertical line Γ_2 moves to the right and tends towards the common vertical asymptote $D = D_1$ for curves Γ_1, Γ_4 and Γ_5, as $S_{2\text{in}}$ tends to S_2^0. In the limit $S_{2\text{in}} = S_2^0$, the very tiny region $\mathcal{I}_3$ (in Yellow on the figure) located between curves Γ_1 and Γ_4, together with $\mathcal{I}_4$ and $\mathcal{I}_5$ regions have disappeared.

For $S_2^0 < S_{2\text{in}} \leq S_2^M$, only regions $\mathcal{I}_0$, $\mathcal{I}_1$, $\mathcal{I}_6$ and $\mathcal{I}_7$ exist. For increasing $S_{2\text{in}}$, the vertical line Γ_2 moves to the right and tends towards Γ_6 as $S_{2\text{in}}$ tends to S_2^M, see Fig. 8(c). For $S_{2\text{in}} > S_2^M$, Γ_3 curve appears, giving birth to $\mathcal{I}_2$ and $\mathcal{I}_8$ regions, see Fig. 8(d). For increasing $S_{2\text{in}}$, the vertical line Γ_3 moves to the left while Γ_5 curve is translated downwards.

It should be noticed that as the case (B), it is seen in Fig. 8 that the region of global asymptotic stability of the positive steady state E_2^1 (the Green region $\mathcal{I}_4 \cup \mathcal{I}_6$) presents the property that there exists a range of values for the operating parameters $S_{1\text{in}}$ and $S_{2\text{in}}$ such that the system can go from the bistability region (the Pink region $\mathcal{I}_5 \cup \mathcal{I}_7$), to the global asymptotic stability region, when the dilution rate D increases.

6   Bifurcations

The surfaces Γ_k, $k = 1 \cdots 6$, are the borders of the regions in the operating parameters space $(D, S_{1\text{in}}, S_{2\text{in}})$ on which bifurcations occur, while the steady states change their stability. In codimension-one bifurcations, only transcritical and saddle node bifurcations can be encountered, as stated in the following result.

Proposition 3. *The bifurcations of the steady states of (2) arising on the boundaries of regions $\mathcal{I}_k$, $k = 0 \cdots 8$, are listed in Table 8.*

Proof. The proof is given in Appendix A.3.   □

Table 8: Codimension-one bifurcations along subsets of surfaces Γ_k and the corresponding cases in [7]: Transcritical bifurcations (TB) and Saddle Node bifurcations (SNB) occur.

Γ_k	Subset of Γ_k	Bifurcation	Case of [7]
Γ_1	$\Gamma_1 \cap \left\{ 0 \leq S_{2\text{in}} < S_2^{1*}(D) \right\}$	TB: $E_1^0 = E_2^0$	
	$\Gamma_1 \cap \left\{ S_2^{1*}(D) < S_{2\text{in}} < S_2^{2*}(D) \right\}$	TB: $E_1^i = E_2^i$, $i = 0, 1$	
	$\Gamma_1 \cap \left\{ S_{2\text{in}} > S_2^{2*}(D) \right\}$	TB: $E_1^i = E_2^i$, $i = 0, 1, 2$	
Γ_2	Γ_2	TB: $E_1^0 = E_1^1$	**1.4, 2.8, 2.9**
Γ_3	Γ_3	TB: $E_1^0 = E_1^2$	**1.5, 2.13**
Γ_4	Γ_4	TB: $E_2^0 = E_2^1$	**2.7**
Γ_5	Γ_5	TB: $E_2^0 = E_2^2$	**2.12, 2.15**
Γ_6 $D_2 < D_1$	$\Gamma_6 \cap \{ 0 \leq S_{2\text{in}} < S_2^M$ and $S_{1\text{in}} > S_1^*(D_2) + \frac{k_1}{k_2}\left(S_2^M - S_{2\text{in}}\right) \}$	SNB: $E_2^1 = E_2^2$	**2.11**
	$\Gamma_6 \cap \left\{ S_{2\text{in}} > S_2^M \text{ and } S_{1\text{in}} > S_1^*(D_2) \right\}$	SNB: $E_j^1 = E_j^2$, $j = 1, 2$	**2.14**
	$\Gamma_6 \cap \left\{ S_{2\text{in}} > S_2^M \text{ and } S_{1\text{in}} < S_1^*(D_2) \right\}$	SNB: $E_1^1 = E_1^2$	**1.6**
Γ_6 $D_1 < D_2$	$\Gamma_6 \cap \left\{ S_{2\text{in}} > S_2^M \text{ and } S_{1\text{in}} > 0 \right\}$	SNB: $E_1^1 = E_1^2$	**1.6**

Remark 3. *The last column of Table 8 shows the corresponding cases with* non hyperbolic *steady states given in Theorem 1 of [7]. The case labeled* **2.10** *in this theorem, where $E_1^0 = E_1^1$ and $E_2^0 = E_2^2$, does not appear in Table 8, since it is a codimension-two bifurcation arising along $\Gamma_2 \cap \Gamma_5$. The bifurcations along Γ_1, corresponding to the condition $S_{1\text{in}} = S_1^*(D)$ were not analyzed in [7]. In Theorem 1 of [7] only the cases $S_{1\text{in}} < S_1^*(D)$ and $S_{1\text{in}} > S_1^*(D)$ were considered.*

To have a better understanding of the nature of the bifurcations of steady states, let us consider the dilution rate D as the bifurcation parameter. Throughout this section, we assume that biological parameters are fixed as in Fig. 7(a),

corresponding to case (b) of Fig. 1 and $S_{2in} = 0$. We now fix the operating parameter S_{1in} at various typical values, as depicted in the horizontal lines shown in Fig. 9, and plot one-parameter bifurcation diagrams in D, with X_i, $i = 1, 2$, on the y-axis, see Fig. 10, 11 and 12.
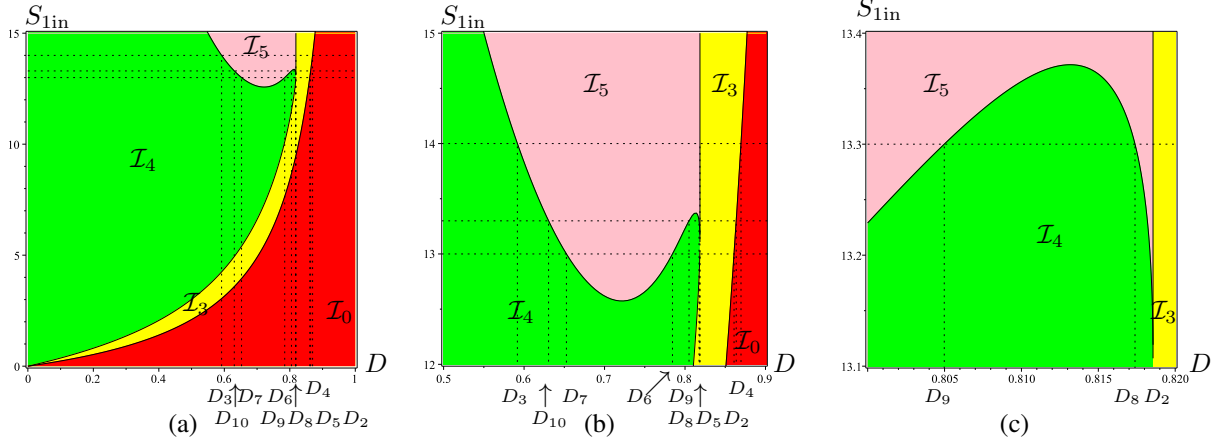

Figure 9: Operating diagram where $S_{2in} = 0$ corresponding to Fig. 7(a). (a): Cuts where S_{1in} is kept constant and D is the bifurcation parameter. (b): Magnification of the operating diagram showing the bifurcation values D_k, defined by (5), (6), and (7). Notice that there are three different values of D_4 corresponding to the three different values $S_{1in} = 13$, $S_{1in} = 13.3$ and $S_{1in} = 14$. (c) : Magnification showing the values $D = D_9$, $D = D_8$ and $D = D_2$.

Recall that the curve Γ_5 separating the Pink and Green regions is the curve of the function $S_{1in} = \frac{k_1}{k_2} H_2(D)$. Case (B) corresponds to a function H_2 which is decreasing, then increasing, then decreasing. For the considered biological parameters values, the function $H_2(D)$ attains its minimum for $D_{min} \simeq 0.72$ and its maximum for $D_{max} = 0.81$ and satisfies $H_2(D_2) = S_2^M + \frac{k_2}{k_1} S_1^*(D_2) \simeq 131.1$, where $D_2 = \frac{1}{\alpha} \mu_2 \left(S_2^M \right) \simeq 0.82$. Therefore, the variations of $\frac{k_1}{k_2} H_2(D)$ are as shown in the following table

D	0		0.72		0.81		0.82
$\frac{k_1}{k_2} H_2(D)$	$+\infty$	$\searrow$	12.57	$\nearrow$	13.37	$\searrow$	13.11

We fix three typical values $S_{1in} = 13$, $S_{1in} = 13.3$ and $S_{1in} = 14$, corresponding to the three horizontal lines shown in Fig. 9. We begin with the case where $S_{1in} = 14$. Since $S_{1in} > 13.37$, as it is seen in Fig. 9, with increasing D, there is a transition from $\mathcal{I}_4$ to $\mathcal{I}_5$ for $D = D_3 \approx 0.5917$, then from $\mathcal{I}_5$ to $\mathcal{I}_3$ for $D = D_2 \simeq 0.8186$, then from $\mathcal{I}_3$ to $\mathcal{I}_0$ for $D = D_4 \simeq 0.8696$. The bifurcation values D_2, D_3 and D_4 are defined by

$$D_4 = \frac{\mu_1(S_{1in})}{\alpha}, \quad D_2 = \frac{\mu_2\left(S_2^M\right)}{\alpha} \quad \text{and } D_3 \text{ is the unique solution of } S_{1in} = \frac{k_1}{k_2} H_2(D) \tag{5}$$

The bifurcation value D_4 corresponds to a transcritical bifurcation of E_2^0 and E_1^0; D_2 corresponds to a saddle node bifurcation of E_2^1 and E_2^2 and D_3 corresponds to a transcritical bifurcation of E_2^0 and E_2^2. The plot of X_1 and X_2 components of all existing steady states with respect of D is shown in Fig. 10. Solid lines and dotted lines correspond to stable and unstable steady states respectively. Since S_{2in} the steady states E_1^1 and E_1^2 cannot exist. On Fig. 10(a), for $0 < D < D_3$, the X_1-component of E_2^i, $i = 0, 2$, is colored in Red, with Green dots, showing the stability of E_2^1 and the instability of E_2^0. For $D_3 < D < D_2$, the X_1-component of E_2^i, $i = 0, 1, 2$, is colored in Red and Green, with Blue dots, showing the bistability of E_2^0 and E_2^1 and the instability of E_2^1. For $D_2 < D < D_4$, the X_1-component of E_2^0 is colored in Green, showing the stability of E_2^0. On Fig. 10(b) and 10(c), for $0 < D < D_2$, the $X_2 = 0$-component of E_j^0, $j = 1, 2$, is colored with Green and Black dots, showing the instability of E_2^0 and E_1^0; For $D_2 < D < D_4$ it is colored in Green, with Black dots, showing the stability of E_2^0 and the instability of E_1^0. For $D > D_4$ it is colored in Black showing the stability of E_1^0

Consider now the case where $S_{1in} = 13$. This case corresponds to the surprising situation where we can go from the bistability region (colored in Pink) to the global asymptotic stability region (colored in Green), when the dilution rate D increases. Since $12.57 < S_{1in} < 13.11$, as it is seen in Fig. 9, with increasing D, there is a transition from $\mathcal{I}_4$ to $\mathcal{I}_5$ for $D = D_7 \approx 0.6526$, then from $\mathcal{I}_5$ to $\mathcal{I}_4$ for $D = D_6 \simeq 0.7844$, then from $\mathcal{I}_4$ to $\mathcal{I}_3$ for $D = D_5 \simeq 0.8184$, then from $\mathcal{I}_3$ to $\mathcal{I}_0$ for $D = D_4 \simeq 0.8609$. The bifurcation values D_4, D_5, D_6 and D_7 are defined by

$$D_4 = \frac{\mu_1(S_{1in})}{\alpha}, \quad D_5 \text{ is the solution of } S_{1in} = \frac{k_1}{k_2} H_1(D), \quad D_6, D_7 \text{ are the solutions of } S_{1in} = \frac{k_1}{k_2} H_2(D) \tag{6}$$
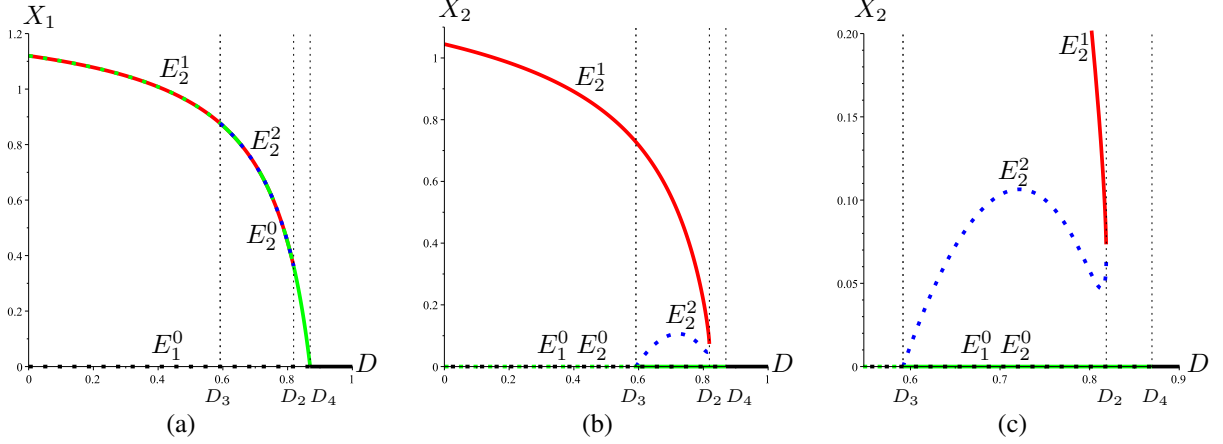
15

Figure 10: Bifurcation diagram with D as the bifurcation parameter, corresponding to Fig. 7(a) and $S_{1in} = 14$. (a): The X_1-components and (b): the X_2-components, of the steady states E_1^0 (in Black), E_2^0 (in Green), E_2^1 (in Red) and E_2^2 (in Blue). (c): A magnification showing the bifurcation values D_1, D_2 and D_3. Solid lines and dotted lines correspond to stable and unstable steady states respectively.
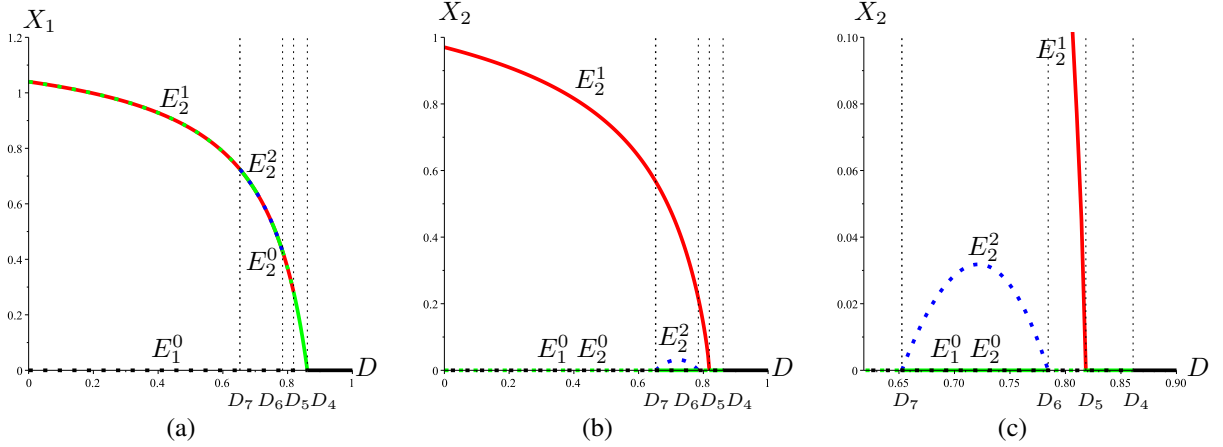

Figure 11: Bifurcation diagram with D as the bifurcation parameter, corresponding to Fig. 7(a) and $S_{1in} = 13$. (a): The X_1-components and (b): the X_2-components, of the steady states E_1^0 (in Black), E_2^0 (in Green), E_2^1 (in Red) and E_2^2 (in Blue). (c): A magnification showing the bifurcation values D_4, D_5, D_6 and D_7. Solid lines and dotted lines correspond to stable and unstable steady states respectively.

The bifurcation value D_4 corresponds to a transcritical bifurcation of E_2^0 and E_1^0; D_5 corresponds to a transcritical bifurcation of E_2^1 and E_2^0 and D_6 and D_7 correspond to transcritical bifurcations of E_2^0 and E_2^2. The plot of X_1 and X_2 components of all existing steady states with respect of D is shown in Fig. 11. Solid lines and dotted lines correspond to stable and unstable steady states respectively. On Fig. 11(a), for $0 < D < D_7$ and $D_6 < D < D_5$ the X_1-component of E_2^i, $i = 0, 2$, is colored in Red, with Green dots, showing the stability of E_2^1 and the instability of E_2^0. For $D_7 < D < D_6$, the X_1-component of E_2^i, $i = 0, 1, 2$, is colored in Red and Green, with Blue dots, showing the bistability of E_2^0 and E_2^1 and the instability of E_2^1. For $D_5 < D < D_4$, the X_1-component of E_2^0 is colored in Green, showing the stability of E_2^0. On Fig. 11(b) and 11(c), for $0 < D < D_7$ and $D_6 < D < D_5$, the $X_2 = 0$-component of E_j^0, $j = 1, 2$, is colored with Green and Black dots, showing the instability of E_2^0 and E_1^0; For $D_7 < D < D_6$ and $D_5 < D < D_4$ it is colored in Green, with Black dots, showing the stability of E_2^0 and the instability of E_1^0. For $D > D_4$ it is colored in Black showing the stability of E_1^0.

Consider now the case where $S_{1in} = 13.3$. This case corresponds also to the situation where we can go from the bistability region (colored in Pink) to the global asymptotic stability region (colored in Green), when the dilution rate D increases. Since $13.11 < S_{1in} < 13.37$, as it is seen in Fig. 9, with increasing D, there is a transition from $\mathcal{I}_4$ to $\mathcal{I}_5$ for $D = D_{10} \approx 0.6304$, then from $\mathcal{I}_5$ to $\mathcal{I}_4$ for $D = D_9 \simeq 0.8050$, then from $\mathcal{I}_4$ to $\mathcal{I}_5$ for $D = D_8 \simeq 0.8173$, then from $\mathcal{I}_5$ to $\mathcal{I}_3$ for $D = D_2 \simeq 0.8186$, then from $\mathcal{I}_3$ to $\mathcal{I}_0$ for $D = D_4 \simeq 0.8636$. The bifurcation values D_2, D_4, D_8, D_9
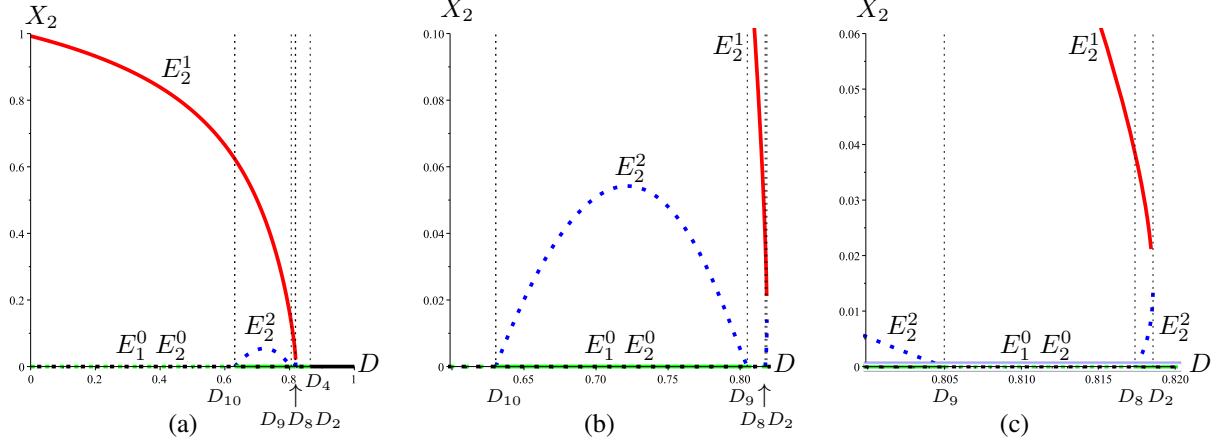
16

Figure 12: Bifurcation diagram with D as the bifurcation parameter, corresponding to Fig. 7(a) and $S_{1\text{in}} = 14$. (a): The X_2-components of the steady states E_1^0 (in Black), E_2^0 (in Green), E_2^1 (in Red) and E_2^2 (in Blue). (b): A magnification showing the bifurcation values D_9 and D_{10}, where D_2 and D_8 are indistinguishable. (c): A larger magnification showing the bifurcation values D_2, D_8 and D_9. Solid lines and dotted lines correspond to stable and unstable steady states respectively.

and D_{10} are defined by

$$D_4 = \frac{\mu_1\left(S_{1\text{in}}\right)}{\alpha}, \quad D_2 = \frac{\mu_2\left(S_2^M\right)}{\alpha} \quad \text{and } D_8, D_9, D_{10} \text{ are the solutions of } S_{1\text{in}} = \frac{k_1}{k_2} H_2(D) \qquad (7)$$

The bifurcation value D_4 corresponds to a transcritical bifurcation of E_2^0 and E_1^0; D_2 corresponds to a saddle node bifurcation of E_2^1 and E_2^2 and D_8, D_9 and D_{10} correspond to transcritical bifurcations of E_2^0 and E_2^2. The plot of the X_2 component of all existing steady states with respect of D is shown in Fig. 12. Solid lines and dotted lines correspond to stable and unstable steady states respectively. Since two magnifications are necessary to represent all bifurcations, the plot of the X_1 component is omitted in Fig. 12. However, it is similar to those plots given in Figs. 10(a) and 11(a). On Fig. 12 for $0 < D < D_{10}$ and $D_9 < D < D_8$, the $X_2 = 0$-component of E_j^0, $j = 1, 2$, is colored with Green and Black dots, showing the instability of E_2^0 and E_1^0; For $D_{10} < D < D_9$ and $D_8 < D < D_4$ it is colored in Green, with Black dots, showing the stability of E_2^0 and the instability of E_1^0. For $D > D_4$ it is colored in Black showing the stability of E_1^0. Notice that for $D_{10} < D < D_9$ and $D_8 < D < D_2$ both steady states E_2^0 and E_2^1 are stable.

7 Discussion

Our main contribution is to present the operating diagram and to show how it depends on the biological parameters.

The parameter space of model (2), where μ_1 and μ_2 are given by (3) is twelve dimensional: nine biological or physical parameters (m_1, m_2, K_1, K_2, K_I, k_1, k_2, k_2 and α) and three operating parameters (D, $S_{1\text{in}}$ and $S_{1\text{in}}$). The former parameters are called biological parameters since they depend on the organisms, and substrate considered. These parameters are measurable in the laboratory. In contrast, the later parameters are called operating parameters since they are under the control of the experimenter.

Exploring all of the twelve dimensional parameter space is almost possible. Fixing the biological parameters and constructing the operating diagram is a powerful answer for the discussion of the behavior of the model with respect of the parameters. Therefore our approach to handle the question of the dependence with respect of the parameters of the model is to split the question in two intermediary questions. First we fix the biological parameters and present the operating diagram. Second we explore how the operating diagram varies when the biological parameters are changed. For instance, Figs. 6, Fig. 7 and Fig. 8 show how the operating diagram changes when the biological parameter m_1 is changed.

The operating diagrams shown in the figures summarize the effect of the operating conditions on the long-term dynamics of the AM2 model and shows six type of behavior: 1) the washout of the two populations (regions colored in Red), 2) the washout of the first population while the second population is maintained (regions colored in Blue), 2) the occurrence of these two behaviors, according to initial conditions (regions colored in Cyan), 4) the washout of the second population while the first is maintained (regions colored in Yellow), 5) the persistence of both populations

(regions colored in Green) and finally 6) the occurrence of these two behaviors according to initial conditions (regions colored in Pink).

In the operating diagrams shown in Figs. 6(a), 7(a) and 8(a), obtained for $S_{2\text{in}} = 0$, only regions $\mathcal{I}_0$, $\mathcal{I}_3$, $\mathcal{I}_4$ and $\mathcal{I}_5$ exist, that is to say, the steady states E_1^i, $i = 1, 2$ without acidogenic bacteria, cannot exist. This property is in accordance with the fact that the system being commensalistic, and without input concentration $S_{2\text{in}}$, it is impossible for the commensal population (the methanogenic bacteria) to survive if the host population (the acidogenic bacteria) is washed out.

The operating diagram shows how robust or how extensive is the parameter region where coexistence occurs, where the corresponding steady state is GAS, where the steady states, with extinction both or one of the population, is stable and where it is unstable.

A Proofs

A.1 Proof of Proposition 1

Table 9: Necessary and sufficient conditions of existence and local stability of the steady states of (2) obtained in [7]. $S_1^*(D)$, $S_2^{i*}(D)$ and $S_{2\text{in}}^*(D, S_{1\text{in}}, S_{2\text{in}})$ are defined in Table 1.

	Existence conditions	Stability conditions
E_1^0	Always exists	$S_{1\text{in}} < S_1^*(D)$ and $S_{2\text{in}} \notin \left[S_2^{1*}(D), S_2^{2*}(D)\right]$
E_1^1	$S_{2\text{in}} > S_2^{1*}(D)$	$S_{1\text{in}} < S_1^*(D)$
E_1^2	$S_{2\text{in}} > S_2^{2*}(D)$	Unstable if it exists
E_2^0	$S_{1\text{in}} > S_1^*(D)$	$S_{2\text{in}}^*(D, S_{1\text{in}}, S_{2\text{in}}) \notin \left[S_2^{1*}(D), S_2^{2*}(D)\right]$
E_2^1	$S_{1\text{in}} > S_1^*(D)$ and $S_{2\text{in}}^*(D, S_{1\text{in}}, S_{2\text{in}}) > S_2^{1*}(D)$	Stable if it exists
E_2^2	$S_{1\text{in}} > S_1^*(D)$ and $S_{2\text{in}}^*(D, S_{1\text{in}}, S_{2\text{in}}) > S_2^{2*}(D)$	Unstable if it exists

The proof follows from [7]. It is seen from Proposition 1 of [7] that the steady states are given by Table 2, where S_1^*, S_2^{i*}, $S_{2\text{in}}^*$, X_1^*, X_2^i and X_2^{i*} are defined in Table 1. The necessary and sufficient conditions of existence of the steady state given in Proposition 1 of [7] are summarized in the second column of Table 9. The necessary and sufficient conditions of local stability of these steady states, obtained in Table A.1 of [7], are summarized in the third column of Table 9.

Let us prove the following result which shows that the existence conditions of X_2^{i*}, $i = 1, 2$ steady states given in Table 9, can be stated using the functions $H_i(D)$, $i = 1, 2$, defined in Table 1. These functions were considered also by [28].

Lemma 1. *The conditions $S_{2\text{in}}^*(D, S_{1\text{in}}, S_{2\text{in}}) = S_2^{i*}(D)$ and $S_{2\text{in}}^*(D, S_{1\text{in}}, S_{2\text{in}}) < S_2^{i*}(D)$, for $i = 1, 2$, are equivalent to the conditions $S_{2\text{in}} + \frac{k_2}{k_1} S_{1\text{in}} = H_i(D)$ and $S_{2\text{in}} + \frac{k_2}{k_1} S_{1\text{in}} < H_i(D)$, for $i = 1, 2$, respectively.*

Proof. The result follows from the definitions of $S_{2\text{in}}^*(D, S_{1\text{in}}, S_{2\text{in}})$ and $H_i(D)$, given in Table 1. Indeed $S_{2\text{in}}^*(D, S_{1\text{in}}, S_{2\text{in}}) = S_2^{i*}(D)$ is equivalent to

$$S_{2\text{in}} + \frac{k_2}{k_1}\left(S_{1\text{in}} - S_1^*(D)\right) = S_2^{i*}(D) \iff S_{2\text{in}} + \frac{k_2}{k_1} S_{1\text{in}} = S_2^{i*}(D) + \frac{k_2}{k_1} S_1^*(D).$$

That is to say $S_{2\text{in}} + \frac{k_2}{k_1} S_{1\text{in}} = H_i(D)$. The proof for the inequality is the same. $\square$

Therefore, the results in Table 9 are equivalent to those in Table 3 which completes the proof of Proposition 1.

A.2 Proof of Proposition 2

The proof follows from [7]. The existence and stability conditions of the steady states of (2) given in Table 9 depend only on the relative positions of the values of S_{1in} and $S_1^*(D)$ and of the values of $S_2^{1*}(D)$, $S_2^{2*}(D)$, S_{2in}, and $S_{2in}^*(D, S_{1in}, S_{2in})$. Actually, as stated in Theorem 1 of [7], we can distinguish nine cases, according to the relative positions of these numbers. These cases are summarized in Table 10.

The cases **1.1**, **1.2** and **1.3** correspond to the regions $\mathcal{I}_0$, $\mathcal{I}_1$ and $\mathcal{I}_2$ respectively, defined in Table 5. Now we use Lemma 1 to show that the remaining six cases **2.1** to **2.6** correspond to the six regions $\mathcal{I}_3$ to $\mathcal{I}_8$ defined in Table 5.

18

Table 10: The 9 cases of existence and stability of steady states of (2) obtianed in [7], where S and U stand for *stable* and *unstable* respectively.

Condition 1	Condition 2	Case	E_1^0	E_1^1	E_1^2	E_2^0	E_2^1	E_2^2
$S_{1\text{in}} < S_1^*(D)$	$S_{2\text{in}} < S_2^{1*}(D)$	**1.1**	S					
	$S_2^{1*}(D) < S_{2\text{in}} \le S_2^{2*}(D)$	**1.2**	U	S				
	$S_2^{2*}(D) < S_{2\text{in}}$	**1.3**	S	S	U			
$S_{1\text{in}} > S_1^*(D)$	$S_{2\text{in}} < S_{2\text{in}}^* < S_2^{1*} < S_2^{2*}$	**2.1**	U			S		
	$S_{2\text{in}} \le S_2^{1*} < S_{2\text{in}}^* \le S_2^{2*}$	**2.2**	U			U	S	
	$S_{2\text{in}} \le S_2^{1*} < S_2^{2*} < S_{2\text{in}}^*$	**2.3**	U			S	S	U
	$S_2^{1*} < S_{2\text{in}} < S_{2\text{in}}^* \le S_2^{2*}$	**2.4**	U	U		U	S	
	$S_2^{1*} < S_{2\text{in}} \le S_2^{2*} < S_{2\text{in}}^*$	**2.5**	U	U		S	S	U
	$S_2^{1*} < S_2^{2*} < S_{2\text{in}} < S_{2\text{in}}^*$	**2.6**	U	U	U	S	S	U

Since $S_{2\text{in}} < S_{2\text{in}}^*$ the case **2.1** corresponds to the condition $S_{2\text{in}}^* < S_2^{1*}$ which is equivalent, using Lemma 1, to $S_{2\text{in}} + \frac{k_2}{k_1} S_{1\text{in}} < H_1(D)$. Therefore the case **2.1** corresponds to the region $\mathcal{I}_3$ defined in Table 5. Using again Lemma 1, the condition $S_2^{1*} < S_{2\text{in}}^* < S_2^{2*}$ in the case **2.2** is equivalent to $H_1(D) < S_{2\text{in}} + \frac{k_2}{k_1} S_{1\text{in}} < H_2(D)$ and the condition $S_{2\text{in}}^* > S_2^{2*}$ in the case **2.3** is equivalent to $S_{2\text{in}} + \frac{k_2}{k_1} S_{1\text{in}} > H_2(D)$. Therefore the cases **2.2** and **2.3** correspond to the regions $\mathcal{I}_4$ and $\mathcal{I}_5$ respectively, defined in Table 5. Using similar arguments we show that the cases **2.4**, **2.5** and **2.6** correspond to the regions $\mathcal{I}_6$, $\mathcal{I}_7$ and $\mathcal{I}_8$ respectively, defined in Table 5.

Excepted for cases **1.3**, **2.3**, **2.5** and **2.6** of bistability, the system (2) has a unique globally asymptotically stable (GAS) steady state. Therefore, in the case **1.1**, E_1^0 is GAS; in the case **1.2**, E_1^1 is GAS, in the case **2.1**, E_2^0 is GAS, and in the cases **2.2** and **2.4**, E_2^1 is GAS. In the case **1.3**, E_1^2 is a saddle point whose attractive manifold is a 3-dimensional hyper-surface surface which separates the phase space of (2) into the basins of attractions of the stable steady states E_1^0 and E_1^1. In the cases **2.3**, **2.5** and **2.6**, E_2^2 is a saddle point whose stable manifold is a 3-dimensional hyper-surface which separates the phase space of (2) into the basins of attractions of the stable steady states E_2^0 and E_2^1. For details and complements on the global behaviour, see section 2.4 of [7]. This completes the proof of Proposition 2.

A.3   Proof of Proposition 3

Part of the proof follows from [7]. It is seen from Theorem 1 of [7] that *non hyperbolic* steady states, that correspond to coalescence of some of the steady state, occur when two (or more) of the values of $S_2^{1*}(D)$, $S_2^{2*}(D)$, S_{2in}, and $S_{2in}^*(D, S_{1in}, S_{2in})$ are equal. Notice that the condition $S_2^{1*}(D) = S_2^{2*}(D)$, arising in cases **1.6**, **2.11** and **2.14** of Theorem 1 of [7], corresponds of the saddle node bifurcations of $E_1^1 = E_1^2$ or $E_2^1 = E_2^2$. This condition holds on Γ_6,

Notice the condition $S_{2\text{in}} = S_2^{1*}(D)$, arising in cases **1.4**, **2.8** and **2.9** of Theorem 1 of [7], corresponds of the transcritical bifurcation $E_1^0 = E_1^1$. This condition holds on Γ_2. Similarly, the condition $S_{2\text{in}} = S_2^{2*}(D)$, arising in cases **1.5** and **2.13** of Theorem 1 of [7], corresponds of the transcritical bifurcation $E_1^0 = E_1^2$. This condition holds on Γ_3.

On the other hand the condition $S_{2\text{in}}^* = S_2^{1*}(D)$, arising in cases **2.7** of Theorem 1 of [7], corresponds of the transcritical bifurcation $E_2^0 = E_2^1$. Using Lemma 1, this condition holds on Γ_4. Similarly, the condition $S_{2\text{in}}^* = S_2^{2*}(D)$, arising in cases **2.12** and **2.15** of Theorem 1 of [7], corresponds of the transcritical bifurcation $E_2^0 = E_2^2$. Using Lemma 1, this condition holds on Γ_5.

Finally we consider the bifurcations occuring when $S_{1\text{in}} = S_1^*(D)$. These bifurcations were not considered in Theorem 1 of [7]. The condition $S_{1\text{in}} = S_1^*(D)$ holds on Γ_1 and corresponds to the transcritical bifurcations $E_1^0 = E_2^0$, $E_1^1 = E_2^1$ and $E_1^2 = E_2^2$. This completes the proof of Proposition 3.

B   Tables

In this section, we give several tables that are used in the paper. In Table 11, we provide the biological parameter values used in the figures. Tables 12 and 13, we give the description of the intersection of the Γ_k surfaces with a two dimesnional operating plane where D or S_{2in} is kept constant respectively. In Table 14, we present the functions defined in Table 1 in the particular case of the Monod and Haldane growth function 3.

Table 11: Nominal parameters values used in [7] and corresponding to the figures.

| Parameter | m_1 | K_1 | m_2 | K_2 | K_I | α | k_1 | k_2 | k_3 |
Unit	d^{-1}	g/L	d^{-1}	mmol/L	mmol/L			mmol/g	mmol/g
Case (A): Figs. 1(a), 2, 3, 6, 9, 10, 11, 12	0.6								
Case (B): Figs. 1(b), 4, 7	0.5	2.1	0.95	24	55	0.5	25	250	268
Case (C): Figs. 1(c), 5, 8	0.4								

Table 12: Intersections of the Γ_k surfaces, $k = 0 \cdots 8$ with a $(S_{1\text{in}}, S_{2\text{in}})$ plane, where D is kept constant.

Γ_k	$\Gamma_k \cap \{D = \text{constant}\}$
Γ_1	Vertical line $S_{1\text{in}} = S_1^*(D)$ if $D < D_1$ Empty if $D \geq D_1$
Γ_2	Horizontal line $S_{2\text{in}} = S_2^{1*}(D)$ if $D \leq D_2$ Empty if $D > D_2$
Γ_3	Horizontal line $S_{2\text{in}} = S_2^{2*}(D)$ if $D \leq D_2$ Empty if $D > D_2$
Γ_4	Oblique line $S_{2\text{in}} + \frac{k_2}{k_1} S_{1\text{in}} = H_1(D)$ if $D < \min(D_1, D_2)$ Empty if $D \geq \min(D_1, D_2)$
Γ_5	Oblique line $S_{2\text{in}} + \frac{k_2}{k_1} S_{1\text{in}} = H_2(D)$ if $D < \min(D_1, D_2)$ Empty if $D \geq \min(D_1, D_2)$
Γ_6	The whole plane if $D = D_2$ Empty if $D \neq D_2$

Acknowledgments

References

[1] N. Abdellatif, R. Fekih-Salem and T. Sari. Competition for a single resource and coexistence of several species in the chemostat. *Mathematical Biosciences and Engineering*, **13** (2016): 631-652. doi:10.3934/mbe.2016012

[2] V. Alcaraz-González, J. Harmand, A. Rapaport, J.P. Steyer, V. González-Alvarez, C. Pelayo-Ortiz, Software sensors for highly uncertain WWTPs : a new approach based on interval observers, *Water Res.* **36** (2002): 2515–2524, doi: 10.1016/S0043-1354(01) 00466-3

[3] V. Alcaraz-González, J. Harmand, A. Rapaport, J.P. Steyer, V. González-Alvarez, C. Pelayo-Ortiz, Application of a robust interval observer to an anaerobic digestion process, *Dev. Chem. Eng. Miner. Process.* **13** (2005): 267-278. doi: 10.1002/apj.5500130308

[4] B. Bar, T. Sari. The operating diagram for a model of competition in a chemostat with an external lethal inhibitor. *Discrete & Continuous Dynamical Systems - B*, **25** (6) (2020): 2093-2120. doi:10.3934/dcdsb.2019203

[5] G. Bastin and D. Dochain. *On-Line Estimation and Control of Bioreactors*. Elsevier Science Publishers, Amsterdam, 1990.

[6] D.J. Batstone, J. Keller, I. Angelidaki, S.V. Kalyuzhnyi, S.G. Pavlostathis, A. Rozzi, W.T.M Sanders, H. Siegrist, V.A. Vavilin. The Iwa Anaerobic Digestion Model No 1 (ADM1). *Water Sci Technol*, **45** (10) (2002): 65–73. doi: 10.2166/wst.2002.0292

[7] B. Benyahia, T. Sari, B. Cherki, J. Harmand. Bifurcation and stability analysis of a two step model for monitoring anaerobic digestion processes. *J. Process Control*, **22** (6) (2012): 1008-1019. doi: 10.1016/j.jprocont.2012.04.012

Table 13: The intersections of the Γ_k surfaces, $k = 0 \cdots 8$ with a $(D, S_{1\text{in}})$ plane, where $S_{2\text{in}}$ is kept constant.

Γ_k	$\Gamma_k \cap \{S_{2\text{in}} = \text{constant}\}$	
Γ_1	Curve of function $S_{1\text{in}} = S_1^*(D)$	
Γ_2	Vertical line $D = \frac{1}{\alpha}\mu_2(S_{2\text{in}})$	if $S_{2\text{in}} \leq S_2^M$
	Empty	if $S_{2\text{in}} > S_2^M$
Γ_3	Vertical line $D = \frac{1}{\alpha}\mu_2(S_{2\text{in}})$	if $S_{2\text{in}} \geq S_2^M$
	Empty	if $S_{2\text{in}} < S_2^M$
Γ_4	Curve of function $S_{1\text{in}} = \frac{k_1}{k_2}(H_1(D) - S_{2\text{in}})$ restricted to the domain $S_{1\text{in}} > S_1^*(D)$	
Γ_5	Curve of function $S_{1\text{in}} = \frac{k_1}{k_2}(H_2(D) - S_{2\text{in}})$ restricted to the domain $S_{1\text{in}} > S_1^*(D)$	
Γ_6	Vertical line $D = D_2$	

Table 14: Auxiliary function in the case given by (3).

$$\mu_1(S_1) = \frac{m_1 S_1}{K_1 + S_1}$$
$$\mu_1(+\infty) = m_1$$
$$S_1^*(D) = \frac{\alpha D K_1}{m_1 - \alpha D}$$
$S_1^*(D)$ is defined for $0 < D < D_1$, where $D_1 = \frac{m_1}{\alpha}$

$$\mu_2(S_2) = \frac{m_2 S_2}{K_2 + S_2 + \frac{S_2^2}{K_I}}$$
$$S_2^M = \sqrt{K_2 K_I}$$
$$\mu_2(S_2^M) = \frac{m_2}{1 + 2\sqrt{K_2/K_I}}$$
$$S_2^{1*}(D) = \frac{(m_2 - \alpha D)K_I - \sqrt{(m_2 - \alpha D)^2 K_I^2 - 4(\alpha D)^2 K_2 K_I}}{2\alpha D}$$
$$S_2^{2*}(D) = \frac{(m_2 - \alpha D)K_I + \sqrt{(m_2 - \alpha D)^2 K_I^2 - 4(\alpha D)^2 K_2 K_I}}{2\alpha D}$$
$S_2^{1*}(D)$ and $S_2^{2*}(D)$ are defined for $0 < D < D_2$, where $D_2 = \dfrac{\mu_2(S_2^M)}{\alpha} = \dfrac{m_2}{\alpha}\dfrac{1}{1 + 2\sqrt{K_2/K_I}}$

$H_i(D) = S_2^{i*}(D) + \frac{k_2}{k_1}S_1^*(D)$, $i = 1, 2$, defined for $0 < D < \min(D_1, D_2)$

$S_{2\text{in}}^*(D, S_{1\text{in}}, S_{2\text{in}}) = S_{2\text{in}} + \frac{k_2}{k_1}S_{1\text{in}} - \frac{k_2}{k_1}S_1^*(D)$, defined for $0 < D < D_1$

$X_2^i(D, S_{2\text{in}}) = \frac{1}{k_3\alpha}(S_{2\text{in}} - S_2^{i*}(D))$, $i = 1, 2$, defined for $0 < D < D_2$

$X_2^{i*}(D, S_{1\text{in}}, S_{2\text{in}}) = \frac{1}{k_3\alpha}(S_{2\text{in}} + \frac{k_2}{k_1}S_{1\text{in}} - \frac{k_2}{k_1}H_i(D))$, $i = 1, 2$, defined for $0 < D < \min(D_1, D_2)$

[8] O. Bernard, Z. Hadj-Sadock, D. Dochain, A. Genovesi, J.-P. Steyer. Dynamical model development and parameter identification for an anaerobic wastewater treatment process. *Biotechnol Bioeng*. **75** (14) (2001): 424-438. doi: 10.1002/bit.10036

[9] A. Bornhöft, R. Hanke-Rauschenbach, K. Sundmacher. Steady-state analysis of the Anaerobic Digestion Model No. 1 (ADM1). *Nonlinear Dynamics*, **73** (2013): 535-549. doi: 10.1007/s11071-013-0807-x

[10] A. Burchard, Substrate degradation by a mutualistic association of two species in the chemostat, *J. Math. Bio.*, **32** (1994): 465-489. doi: 10.10 07/BF0 0160169

[11] Y. Daoud, N. Abdellatif, T. Sari, J. Harmand, Steady state analysis of a syntrophic model: The effect of a new input substrate concentration, *Math. Model. Nat. Phenom.*, **13** (3) (2018): 31. doi: 10.1051/mmnp/2018037

[12] M. Dellal, M. Lakrib, T. Sari. The operating diagram of a model of two competitors in a chemostat with an external inhibitor. *Mathematical Biosciences*, **302** (2018): 27-45. doi: 10.1016/j.mbs.2018.05.004

[13] M. El-Hajji, F. Mazenc, J. Harmand, A mathematical study of a syntrophic relationship of a model of anaerobic digestion process, *Mathematical Biosciences & Engineering*, **7** (3) (2010): 641-656. doi: 10.3934/mbe.2010.7.641

[14] R. Fekih-Salem, C. Lobry and T. Sari. *A density-dependent model of competition for one resource in the chemostat*, *Mathematical Biosciences*, **286** (2017): 104-122. doi: 10.1016/j.mbs.2017.02.007

[15] M.J. De Freitas and A.G. Fredrickson, Inhibition as a factor in the maintenance of the diversity of microbial ecosystems, *Journal of General Microbiology*, **106** (1978): 307-320. doi: 10.1099/00221287-106-2-307

[16] C. García-Diéguez, O. Bernard and E. Roca. Reducing the Anaerobic Digestion Model No.1 for its application to an industrial wastewater treatment plant treating winery effluent wastewater, *Bioresource Technology*, **132** (2013): 244-253. doi: 10.1016/j.biortech.2012.12.166

[17] M. Hanaki, J. Harmand, Z. Mghazli, A. Rapaport, T. Sari, P. Ugalde. Mathematical study of a two-stage anaerobic model when the hydrolysis is the limiting step (2020). hal-02531141v2

[18] J. Harmand, A. Rapaport, D. Dochain. How increasing removal rate can globally stabilize the anaerobic digestion model (2020). hal-02549669

[19] J. Harmand, C. Lobry, A. Rapaport and T. Sari, *The Chemostat: Mathematical Theory of Microorganism Cultures*, Wiley ISTE Editions, 2017.

[20] J.L. Jost, J.F. Drake, A.G. Fredrickson, H.M. Tsuchiya. Interactions of *Tetrahymena pyriformis, Escherichia coli, Azotobacter Vinelandii*, and glucose in a minimal medium. *J. Bacteriol.*, **113** (2) (1973): 834-840. PMCID: PMC285298

[21] Z. Khedim, B. Benyahia, B. Cherki, T. Sari, J. Harmand, Effect of control parameters on biogas production during the anaerobic digestion of protein-rich substrates, *Applied Mathematical Modelling*, **61** (2018), 351–376. doi: 10.1016/j.apm.2018.04.020

[22] J. Monod, La technique de culture continue. Théorie et applications, *Annales de l'Institut Pasteur*, **79** (1950): 390-410. doi: 10.1016/B978-0-12-460482-7.50023-3

[23] S. Pavlou, Computing operating diagrams of bioreactors, *J. Biotechnol.* **71** (1999): 7-16. doi: 10.1016/s0168-1656(99)00011-5

[24] P.J. Reilly (1974), Stability of commensalistic systems, *Biotechnology and Bioengineering* **16** (1974): 1373-1392. doi: 10.1002/bit.260161006

[25] T. Sari, M. El-Hajji, J. Harmand, The mathematical analysis of a syntrophic relationship between two microbial species in a chemostat, *Math. Biosci. Eng.*, **9** (2012): 627-645. doi: 10.3934/mbe.2012.9.627

[26] T. Sari and J. Harmand. A model of a syntrophic relationship between two microbial species in a chemostat including maintenance. *Mathematical Biosciences*, **275** (2016): 1-9. doi: 10.1016/j.mbs.2016.02.008

[27] T. Sari, M.Wade, Generalised approach to modelling a three-tiered microbial food-web, *Math. Biosci.*, **291** (2017): 21-37. doi: 10.1016/j.mbs.2017.07.005

[28] M. Sbarciog, M. Loccufier, E. Noldus. Determination of appropriate operating strategies for anaerobic digestion systems. *Biochemical Engineering Journal*, **51** (2010): 180-188. doi: 10.1016/j.bej.2010.06.016

[29] H.L. Smith and P. Waltman, *The theory of the chemostat: Dynamics of microbial competition*, Cambridge University Press, 1995.

[30] G. Stephanopoulos, The dynamic of commensalism, *Biotechnology and Bioengineering* **23** (1981): 2243-2255. doi: 10.1002/bit.260231008

[31] M.J. Wade, J. Harmand, B. Benyahia, T. Bouchez, S. Chaillou, B. Cloez, J.-J. Godon, B. Moussa Boudjemaa, A. Rapaport, T. Sari, R. Arditi and C. Lobry, Perspectives in mathematical modelling for microbial ecology. *Ecological Modelling* **321** (2016): 64-74. doi: 10.1016/j.ecolmodel.2015.11.002

[32] M. Wade, R. Pattinson, N. Parker, and J. Dolfing, Emergent behaviour in a chlorophenol- 597 mineralising three-tiered microbial 'food web', *J. Theor. Biol.*, **389** (2016): 171-186. doi: 0.1016/j.jtbi.2015.10.032

[33] M. Weedermann, G. Seo, G. Wolkowics, Mathematical Model of Anaerobic Digestion in a Chemostat: Effects of Syntrophy and Inhibition, *Journal of Biological Dynamics* **7** (2013): 59-85. doi: 10.1080/17513758.2012.755573

[34] M. Weedermann, G. Wolkowicz, J. Sasara, Optimal biogas production in a model for anaerobic digestion. *Nonlinear Dynamics* **81** (2015): 1097-1112. doi: 10.1007/s11071-015-2051-z

[35] A. Xu, J. Dolfing, T. Curtis, G. Montague, and E. Martin, Maintenance affects the stability of a two-tiered microbial 'food chain'?, *J. Theor. Biol.*, **276** (2011), 35-41. doi: